Methods for Controlling Structure and Photophysical Properties in Polyfluorene Solutions and Gels

ARTICLE *in* ADVANCED MATERIALS · FEBRUARY 2013

Impact Factor: 17.49 · DOI: 10.1002/adma.201204296 · Source: PubMed

2 AUTHORS:

Matti Knaapila
Technical University of Denmark
86 PUBLICATIONS **1,602** CITATIONS
SEE PROFILE

Andy Monkman
Durham University
416 PUBLICATIONS **9,825** CITATIONS
SEE PROFILE

REVIEW

Methods for Controlling Structure and Photophysical Properties in Polyfluorene Solutions and Gels

Matti Knaapila and Andrew P. Monkman**

Knowledge of the phase behavior of polyfluorene solutions and gels has expanded tremendously in recent years. The relationship between the structure formation and photophysics is known at the quantitative level. The factors which we understand control these relationships include virtually all important materials parameters such as solvent quality, side chain branching, side chain length, molecular weight, thermal history and myriad functionalizations. This review describes advances in controlling structure and photophysical properties in polyfluorene solutions and gels. It discusses the demarcation lines between solutions, gels, and macrophase separation in conjugated polymers and reviews essential solid state properties needed for understanding of solutions. It gives an insight into polyfluorene and polyfluorene beta phase in solutions and gels and describes all the structural levels in solvent matrices, ranging from intramolecular structures to the diverse aggregate classes and network structures and agglomerates of these units. It goes on to describe the kinetics and thermodynamics of these structures. It details the manifold molecular parameters used in their control and continues with the molecular confinement and touches on permanently cross-linked networks. Particular focus is placed on the experimental results of archetypical polyfluorenes and solvent matrices and connection between structure and photonics. A connection is also made to the mean field type theories of hairy-rod like polymers. This altogether allows generalizations and provides a guideline for materials scientists, synthetic chemists and device engineers as well, for this important class of semiconductor, luminescent polymers.

1. Introduction

Even though the community has been working on π-conjugated macromolecules for more than half a century, an in-depth intermolecular structural understanding did not emerge until the 80s and 90s when Winokur, Tashiro and others began to publish detailed X-ray scattering data of polymers such as polythiophene,[1] polyacetylene,[2] polyaniline,[3] polyphenylene vinylene,[4] polyfluorene,[5] and polypyridine[6] in the solid state. Over the following decades these studies were followed by several overlapping processes of direct structural studies. One line focused on ever increasing sophistication in details and experimental methods, as followed for example by Winokur, Brinkmann, ourselves and others.[7] A second line focused on increasingly complicated materials and their combinations, dopants and intercalates, as shown by Winokur and others,[8] bringing its motivation from the hydrogen bonded π-conjugated materials,[9] their supramolecular assemblies,[10] nanocomposites[11] and blends,[12] for example. A third line concerned the optimization of structure-property relationships *vis-à-vis* thin film devices, as pioneered for example by Nielsen, Toney, Kline, McGehee and others.[13]

A further apparent research line was also finding structure property relationships for π-conjugated materials in solvent matrices, where the state of material varies from solutions to lyotropic liquid crystals, gels and colloids, as pioneered by Fytas and others.[14] This research line borrows much from the solid state studies since the demarcation lines between these systems, solutions, liquid crystals and gels, are mostly indistinct and what is called as solution may contain polymer aggregates of various kinds including crystallites. In general, polymer gels contain time-dependent and time-independent spatial fluctuations,[15] the former appearing as liquid-like and the latter as solid-like. Ultimately, the aggregates growing from the seemingly isotropic solutions may be connected via permanent covalent bonds; or they may contain charged groups forming strong connections via charge transfer in a liquid matrix.

Initially, a major effort, studying the solution structures in π-conjugated polymers was placed on the para-coupled phenylene type polymers such as poly(*p*-phenylene)s (PPPs) and pioneered by Wegner, Ballauff, Fytas and coworkers.[16] These studies were primarily motivated by the conformational studies of hairy-rod type polymers in general.[17] However, since poly(*p*-phenylene vinylene) (PPV) type polymers had revolutionalized polymer science by paving the way to the polymer based light emitting diodes by Friend et al.,[18] it is not a surprise that the focus shifted towards clarifying connections between structural and opto-electronic properties, for example by Perahia, Traiphol

Dr. M. Knaapila
Physics Department
Institute for Energy Technology
2027 Kjeller, Norway
E-mail: matti.knaapila@ife.no
Prof. A. P. Monkman
Department of Physics
Durham University
Durham DH1 3LE, UK
E-mail: a.p.monkman@durham.ac.uk

DOI: 10.1002/adma.201204296

and Bunz and others for poly(*p*-phenylene ethylene) (PPE) type polymers[19,20] and Chen and others for PPV type polymers.[21,22] Based on the combined structural and optical studies the scientists identified three general tendencies. First, in dense solutions, phenylene type polymers manifest aggregate networks with complicated structural hierarchy and physically bonded nodes, as shown in **Figure 1**. Second, this kind of aggregation is driven by decreasing temperature as illustrated for PPE in toluene in **Figure 2**. Third, the aggregation is driven by poorer solvent, such as adding nonane to the isotropic PPV toluene solution.[23]

This process was followed by a rich variety of other polymers including blue emitting polyfluorene polymer introduced in the 90s by Fukuda and others.[24] Polyfluorenes represent a major materials class and an exceedingly rich research topic. They serve as a first class blue emitter in PLED applications[25] and their opto-electrical properties can be endlessly varied by introducing heterocycles and metals.[26] They also constitute a hairy-rod polymer a model for phase behavioral studies.[27,28] Much of the recent progress in the fundamentals of materials science of polyfluorenenes concerned its intra and intermolecular structures[29] and their relation to their complex photophysical properties[30] but the polyfluorene solutions and gels deserve particular attention. These materials follow similar tendencies to phenylene type polymers but unusually have many structural and optical variants, much of this stemming from their complicated polycrystallinity in the solid state. They show a peculiar β-phase not commonly found in for other π-conjugated macromolecules. They have not been studied systematically until fairly recently but the recent quantitative methods have raised this field quickly to the advanced state. To date this research has not been summarized.

In this paper, we provide a review of the state of the art of the structure and photophysics in polyfluorene solutions and gels. We focus on a neutral and physically cross-linked system thus largely omitting conjugated polyelectrolytes and permanently chemically cross-linked systems. Moreover, we focus on the materials aspects without going into the details of their applications in organic electronics. First, we list key properties of the solid state polyfluorene. Second, we introduce its structural levels in solvent matrices using structural archetypes which allow the greatest possible generalizations, but also paying particular attention on the archetypical toluene and methylcyclohexane (MCH) matrices. Third, we discuss temporal and thermal constraints in these systems. We then detail the molecular parameters that control this behavior. Finally, we move on to selected intriguing closely related systems, where the lessons can be applied, finally making the conclusion of their impact.

Matti Knaapila obtained his Dr. Tech. from the Helsinki University of Technology. He conducted research at the University of Helsinki, at the University of Durham and at MAX-lab, Lund University, before moving to the Institute for Energy Technology in 2008. His research fields include the structure and phase behavior of luminescent polymers and conjugated polyelectolyte-surfactant systems. Knaapila is an expert in the use of synchrotron radiation and neutron scattering.

Andrew Monkman obtained his PhD from the University of London. In 1988 he became lecturer in Molecular Electronics and 2002 Professor of Physics at the University of Durham. Prof. Monkman is the director of the Durham Photonic Materials Center. His current research themes range from femtosecond laser spectroscopy, triplet exciton dynamics and lasing in luminescent polymers to the development of novel phosphorescent materials and spectroscopic measurements of materials in OLED devices.

2. Structure and Photophysical Properties of Polyfluorene in the Solid State

In order to understand polyfluorene solutions and gels, they should mirror isolated polymers and the solid state. In this context, much can be learnt by considering the relation between structural and optical properties of the archetypical branched side chain poly[9,9-bis(2-ethylhexyl)fluorene-2,7-diyl] (PF2/6) and linear side chain poly(9,9-dioctylfluorene) (PFO or PF8) and their various analogues, see their chemical structures in Figure 3.

When isolated, individual polymer chains are concerned, PF2/6[31,32] has been found to adopt a helical main chain conformation with largely disordered side chains. PF8 main chain can be understood in terms of conformational isomers defined by the torsional angle between the repeat units and classified as C_α (torsional angle ~135°), C_β (~160°), and C_γ (~150°) families,[33,34] the beta family containing a single member only. Another classification can be made between the disordered glassy phase and weakly ordered planar β-phase, the latter corresponding to the introduced beta conformer.[35] While the details of the models may vary, there is a consensus that the β-phase involves planarization of the main chain as proposed first by Cadby et al.[36]

When the solid state structure is concerned, PF2/6[32,37] and its oligomeric analogues[31,38,39] always assume a 21-helical main chain conformation. For polydisperse polymer this leads to a hexagonal phase which turns to nematic with increasing temperature and decreasing molecular weight.[27,28] Monodisperse oligomers remain crystalline.[38] The hexagonal structure consists of ensembles of three chains (Figure 4a) and the crystallites form a mosaic of distinct orientation classes in

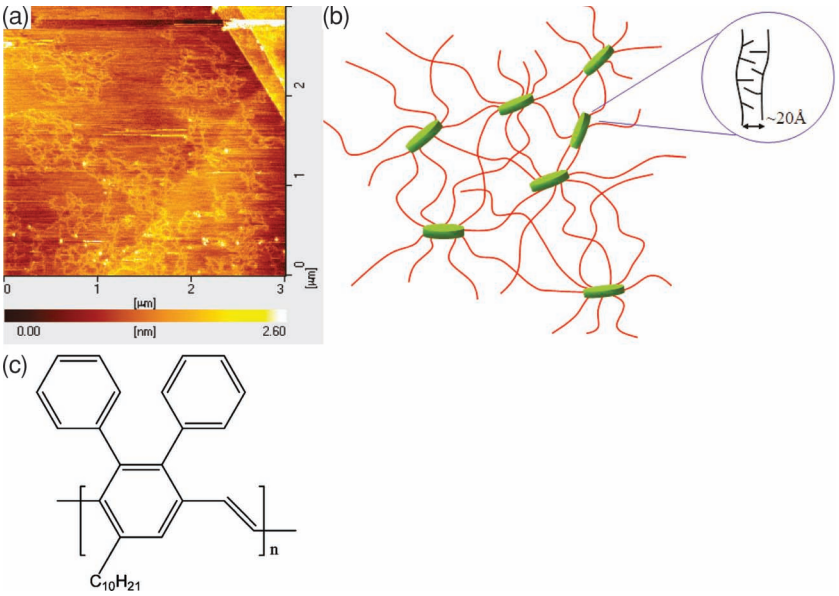

Figure 1. (a) AFM topographic image of poly(2,3-diphenyl-5-decyl-1,4-phenylenevinylene) (DP10-PPV) cast form chloroform solution. (b) Schematics of the DP10-PPV aggregates in toluene. (c) Chemical structure of DP10-PPV. Reproduced with permission.[22] Copyright 2009, the American Chemical Society.

thin aligned films.[40] PF8 is significantly polycrystalline exhibiting crystalline structures[41] including crystalline α-phase and metastable α'-phase and a series of noncrystalline phases[42] including nematic, glassy and amorphous and isotropic phases and so called β-phase, which even though called a noncrystalline phase, gives rise to Bragg reflections. These phases can coexist to various degrees, depending on thermal history.[42] Solid state PF8 shows an order disorder transition (ODT) from any ordered or weakly ordered phase (including the β-phase) to an isotropic phase at about 80 °C.[43] The phase content depends furthermore on solvent treatment such that the β-phase is favored by swelling in a vapor of poor solvents. The β-phase content is always relatively low and it possibly never dominates the material. Various models including a zig-zag,[5] orthorhombic[44] and biradial and tetraradial constructions[45] (Figure 4b-d) have been proposed for the α-phase. Although known in less detail, similar but not identical polycrystallinity is observed for other linear side chain polyfluorenes such as poly(9,9-dihexylfluorene) (PF6)[46] and poly(9,9-diheptylfluorene) (PF7).[47]

When the photophysical properties of polyfluorenes are concerned[30] the solid state phases show different and coexisting optical fingerprints. The β-phase was reported first by Grell[48] as a narrow emission band red-shifted 100 meV from those seen in the glassy polymer. This observation should be taken as its fundamental definition even though a term phase might refer better to its structural manifestation. The optical properties of this phase have been elaborated in great detail[49,50] and similar characteristics have been found for other solid state materials, most particularly for oligofluorenes.[51] Also lasing has been developed based on the β-phase.[49,52,53] Figure 5 shows examples of photoabsoption and photoluminescence data for various states of solid state PF8. The notation used by Grell and coworkers refers elsewhere to glassy (Figure 5a) and nematic phases (Figure 5b) and the crystalline α-phase (Figure 5c) and mesomorphic (or weakly crystalline) β-phase (Figure 5d).

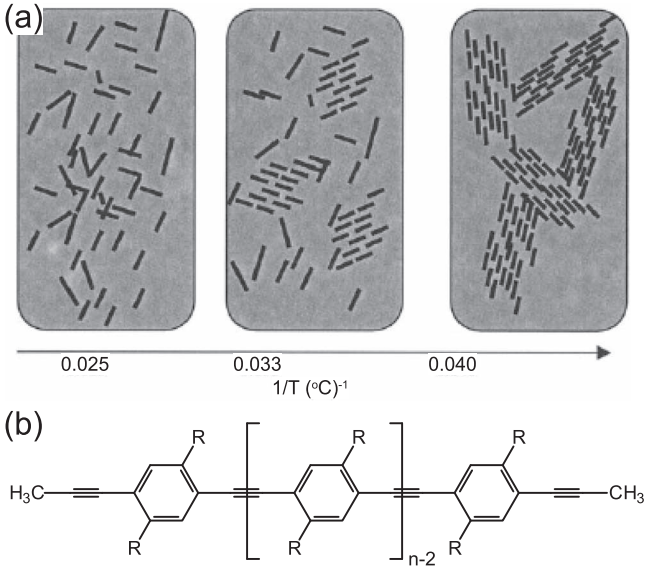

Figure 2. (a) Schematics of the aggregation process of dialkyl poly(*p*-phenylene ethylene) (PPE) in toluene. (b) Chemical structure of dialkyl PPE. Reproduced with permission.[20]

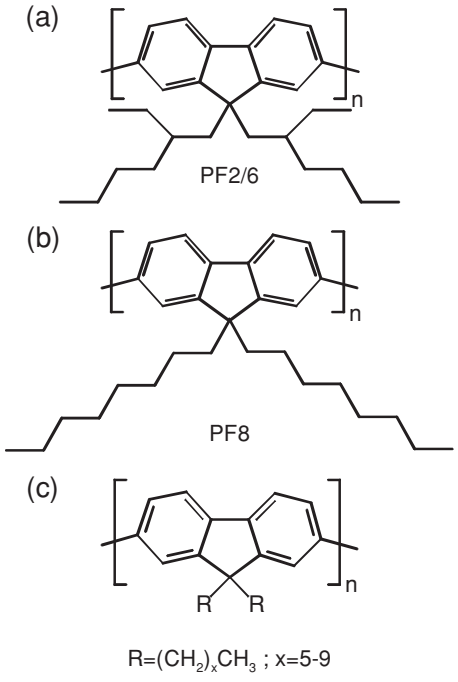

Figure 3. Chemical structures of (a) PF2/6, (b) PF8 and (c) PFs with the linear side chains containing from 6 to 10 carbon atoms.

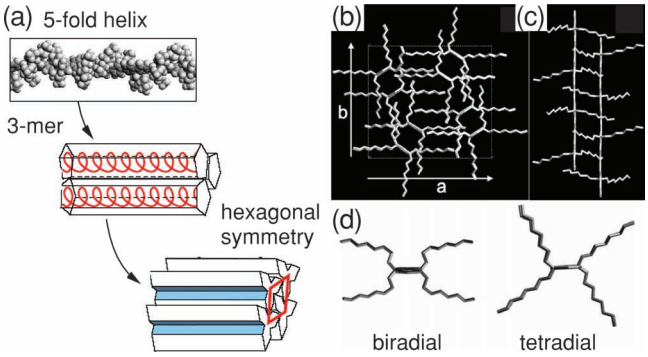

Figure 4. (a) Structural hierarchy of solid state PF2/6. Adapted.[29] (b) The *c*-axis projection (parallel to the polymer backbone) of the refined PF8 crystal structure. (c) Corresponding projection of the two-chain pattern along the 110 direction. (d) Projections of the PF8 chain conformation along the *c*-axis for the biradial and tetradial configuration of the *n*-octyl side chains. Hydrogen atoms are omitted for clarity. Reproduced with permission.[45] Copyright 2007, the American Chemical Society.

3. Structural Levels in Dense Polyfluorene Solutions and Gels

3.1. Archetypical Polyfluorene Mixtures

The essence of polyfluorene solutions and gels may be learnt by considering the PF2/6 and PF8 in toluene and MCH. Toluene is considered a fairly good solvent for the main chain and a fairly poor solvent for the side chains and was first introduced in a structural context by Grell et al.[48] and Fytas et al.[54] MCH is considered a fairly poor solvent for both main and side chains and was originally introduced in the context of thermal behaviour and optical effects by Dias et al.[55] and in the structural context by us.[56] A large number of papers followed these reports and numerous polyfluorene variants in toluene and MCH were introduced.

3.2. Well Dissolved Polyfluorene Chains In Solution

The polymer interaction can be characterized by the overlapping (chain) concentration $c^* \sim N R_g^{-d}$. This concentration can be calculated in various ways depending on polymer geometry[57] but it general increases with increasing degree of polymerization, N, and with decreasing radius of gyration, R_g. Phenomenologically speaking, the dilute mixtures ($c<c^*$) appear visually as transparent liquids, the dense mixtures ($c>c^*$) appear rather as honey-like gels.

Fytas and coworkers[54] studied dissolved polyfluorene chains in solutions and presented elegant light scattering studies of PF2/6 polymers in a dilute toluene thus describing their rotation and translational diffusion dynamics. The authors considered solutions whose concentration was below c^*. They proposed that the corresponding single, nominally isolated and non-interacting PF2/6 polymers are understood best as worm-like fuzzy cylinders with the persistent length 7 ± 0.5 nm and a cross section diameter of ~2 nm.

3.3. Networks of Polyfluorene Chains in Solution

Elsewhere, Chen and coworkers[58] and Justino et al.[59] studied the entanglement process of PF8 in toluene. When the concentration is less than c^*,[60] the PF8 chains are understood as isolated stiff polymers which bend over the distances above their persistence length ~8.5 nm.[48] However, when the concentration exceeds c^* (>0.2 mg/mL), polymers tend to overlap forming a network structure. The mesh size of such network is of the order of 10 nm depending on PF8 concentration. Furthermore, when the concentration is raised higher still (>30 mg/mL), some parts of these chains form aggregate domains within the overlapping polymers such that the average distance between domains is 50-60 nm (Figure 6). This process is driven by π–π interactions between polymer backbone and toluene molecules. The aggregate domains formed in these gels resemble lyotropic liquid crystals such that they do not possess a crystalline order and the emerging network is dynamic rather than rigid. As the chain entities participating in these aggregate domains are relatively short, they appear rodlike and tend to align with the other participating parts. This fact justifies a term "segmental alignment" coined by Chen et al.[58]

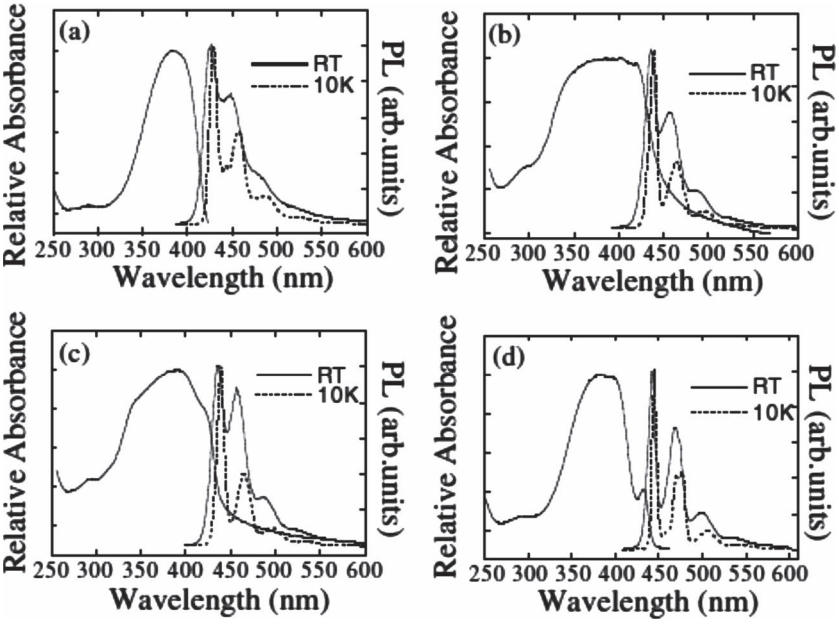

Figure 5. The room temperature and 10 K absorption and PL spectra for PF8 in different morphologies. (a) as spin coated glass. (b) Quenched nematic glass. (c) Crystalline. (d) Toluene vapour-treated spin coated glass with a fraction of β-chains. Reproduced with permission.[94] Copyright 2002, the Institute of Physics.

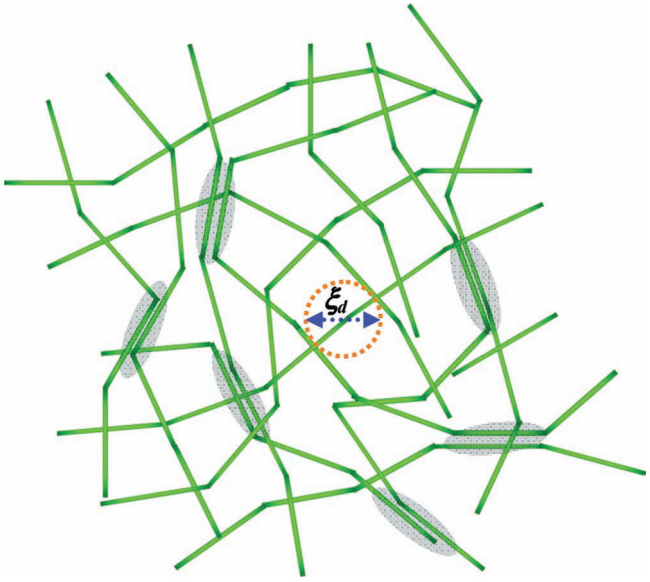

Figure 6. Highly concentrated PF8 network in a good solvent toluene. Shaded areas mark segmental aligned aggregate domains whereas ξ_d marks the mesh size of overlapping chains. Reproduced with permission.[58] Copyright 2007, the American Chemical Society.

3.4. Nanocrystallites in Solution

While Chen and co-workers introduced segmental alignment, we studied polyfluorenes in ~1% MCH mixtures and shown the existence of nano-scaled crystallites.[61] Figure 7 shows room temperature wide-angle X-ray scattering (WAXS) data of these structures for linear side chain PF6, PF7, PF8, poly(9,9-dinonylfluorene) (PF9) and poly(9,9-didecylfluorene) (PF10). Apart from PF10 the data contain sharp X-ray reflections pointing to the ordered, crystalline domains. As these peaks cannot be observed without careful removal of the solvent background, these domains are clearly a minority compound. Likewise, the material appears as a gel but not liquid or solid.

PF8/MCH shows a sharp peak at 0.47 $Å^{-1}$ which can be indexed as 200.[61] This peak and its multiplicities stem from the structure which corresponds to the β-phase in the solid state.[42] PF7 and PF9 show similar albeit not identical peaks. PF7, PF8 and PF9 show the optical fingerprint of β-phase both for 10 mg/mL (i.e. above c^*)[61] and 7 µg/mL (i.e. below c^*)[62] mixtures. The crystalline structure present in PF6/MCH differs from the β-phase which is not observed optically either. PF10 appears isotropic but this holds only for room temperature and the polymer organize on cooling (vide infra).

The crystallites in PF/MCH are much better ordered than the aggregate domains in PF8/toluene which show the characteristics of segmental alignment. The origin of this order can be attributed to the poorer MCH solvent. This tendency appears fairly general amongst π-conjugated polymers. Elsewhere, Chiu and Chen[63] studied poly[2-methoxy-5-(2-ethylhexyloxy)-1,4-phenylenevinylene] (MEH-PPV) in trinary toluene nonane mixture and shown segmental association of MEH-PPV aggregates in toluene but emerging crystalline order leading to the WAXS peaks when the fraction of poorer solvent nonane is increased up to 30%.

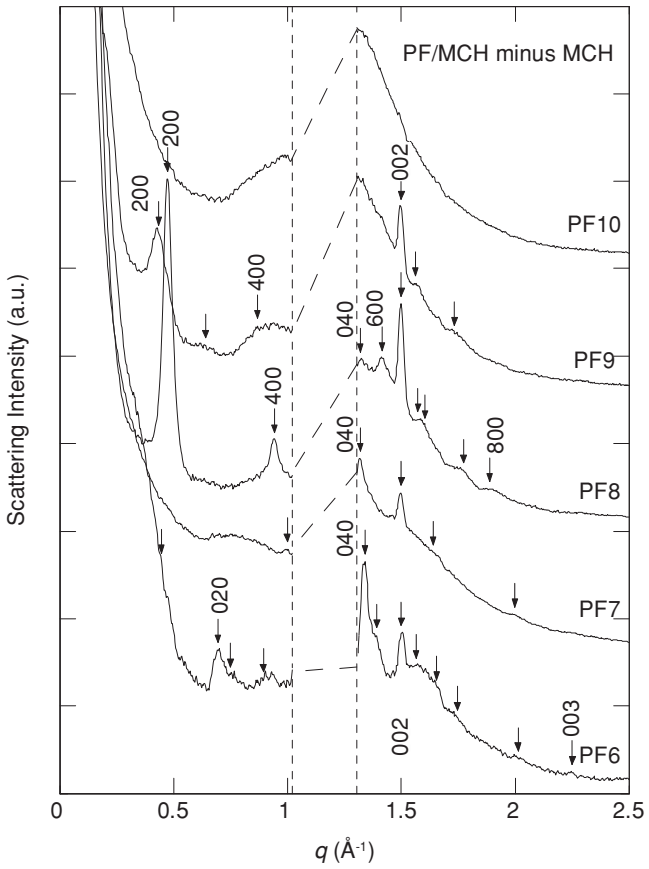

Figure 7. WAXS data of linear side chain polyfluorenes in MCH. The MCH background is subtracted and the curves shifted for clarity. The dashed vertical lines show a q-range which should not be considered. Reproduced with permission.[61] Copyright 2007, the American Chemical Society.

3.5. Sheetlike Aggregates in Solution

When working on the polyfluorene solutions and gels, one of our initial objectives was to clarify nanometer scale solution structure in PF8/MCH. For this reason we studied PF8 in dense ~1% mixtures of deuterated MCH (MCH-d_{14}) using small-angle neutron scattering (SANS) and observed well-defined sheet-like aggregates.[56] We subsequently extended these studies to other polyfluorene polymers. Figure 8 shows SANS data of a series of linear side chain polyfluorenes in MCH-d_{14}. The study shows that the nature of these sheets can vary from polymer to polymer and different sheet types can coexist.[64,65] In general, the sheets are a few nanometers thick but they reach laterally over tens of nanometers.[61] In Figure 8, the letters a and b mark the data corresponding to these extremes. The sheets can be so thin that they are essentially polymer bilayers which we denoted as "membranes". The membranes are liquid crystalline like and weakly ordered. The sheets can also be thicker and for example for PF9, several polymer layers give rise to a weak interference maximum[61] marked by a letter c in Figure 8. The sheets can (but do not have to) manifest the optical and crystallographic fingerprint of the β-phase. The sheets contain primarily only

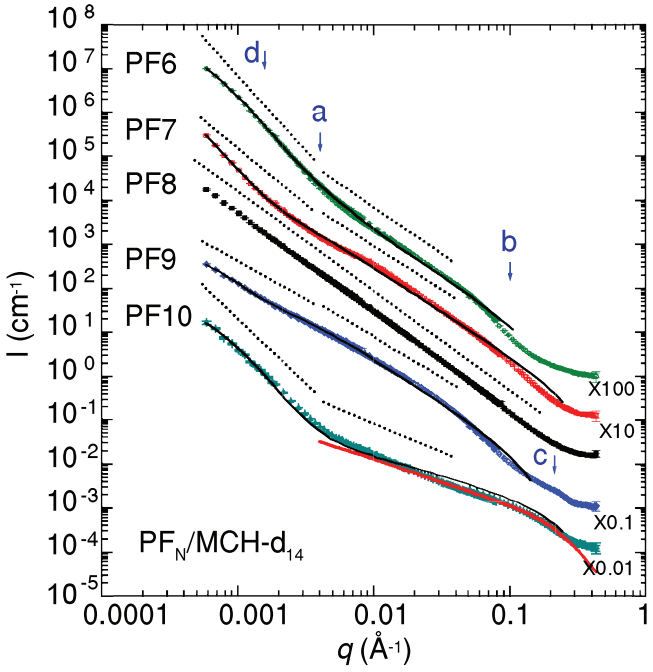

Figure 8. SANS data of linear side chain polyfluorenes in MCH-d_{14}. Arrows mark the approximate q-ranges associated with the lateral size, a, and thickness of the sheet, b, an interference maximum, c, and the network of sheets, d. Reproduced with permission.[65] Copyright 2011, the American Physical Society.

one crystallite type and we expect that the β-phase is primarily present in the crystallites.

3.6. Agglomerates of Sheetlike Aggregates

The observed sheetlike polyfluorene aggregates in MCH overlap and form networking ribbonlike agglomerates.[65] In **Figure 8**, the letter d marks the scattering which stems from these kinds of agglomerates. **Figure 9** shows a TEM image

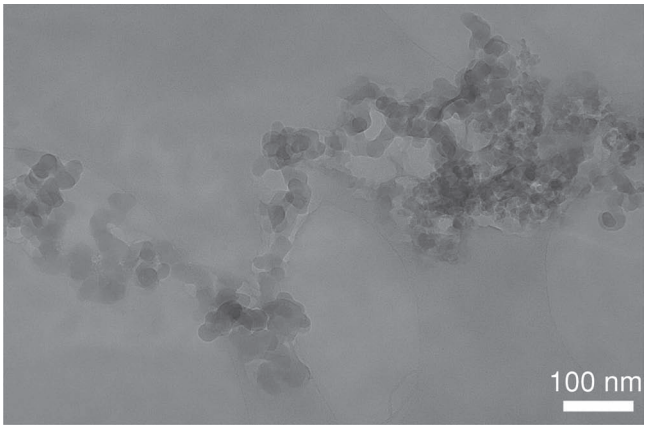

Figure 9. A TEM image of agglomeration of sheetlike PF7 aggregates cast from MCH. The scale bar is 100 nm. Image courtesy of Fredrik Hage, Institute for Energy Technology.

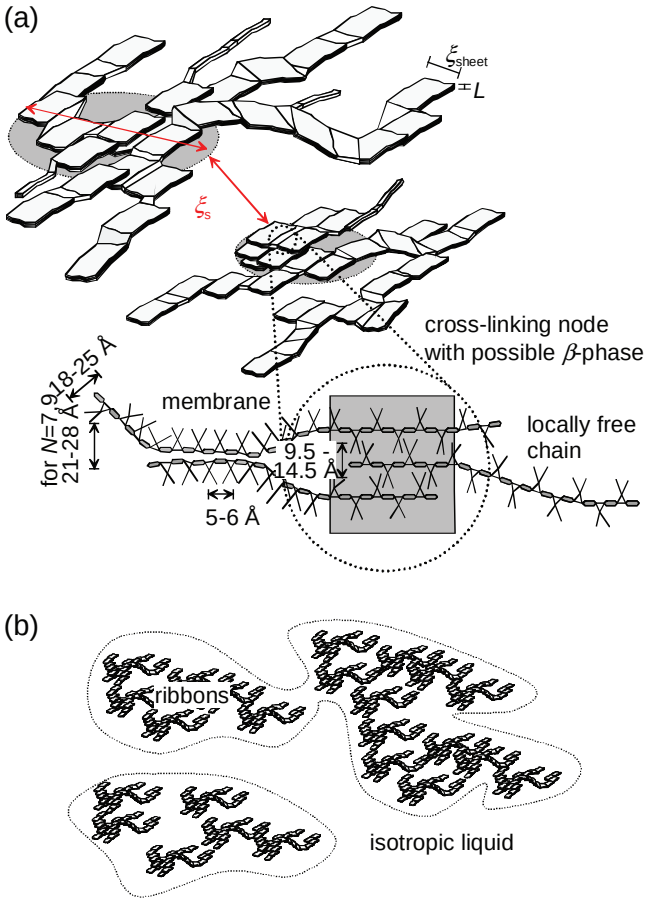

Figure 10. (a) Ribbonlike agglomerates of sheetlike polyfluorene aggregates. The ribbons can contain loose membranes, weakly ordered cross-linking areas and to certain extent locally free chains. (b) Separation of ribbon rich domains and isotropic liquid. Adapted with permission .[65] Copyright 2011, the American Physical Society.

of an agglomerate of sheetlike aggregates deposited on a surface. **Figure 10**a summarizes the proposed relation between agglomerates, sheetlike aggregates, 2-dimensional crystallites and separated polymer chains. The sheetlike aggregates can be thick and ordered or primarily thin bilayers denoted as membranes.[64] The crystallites are clearly a minority compound as are the segmental aggregate domains in PF8/toluene mixtures. Similarly, the polyfluorene crystallites are expected to act as nodes in the physical network of sheetlike aggregates. These ordered crystalline nodes may contain the β-phase for PF8 and an equivalent phase for PF7 and PF9 whereas PF6 contains an ordered sheetlike structure which does not show the optical fingerprint of the β-phase. All samples are likely to contain separated polymer chains. The areas of agglomerates are macroscopically uniform but these systems may become separated into the domains of ribbon like agglomerates within the solvent coexisting with the isotropic liquid. This phenomenon is illustrated in Figure 10b.

Interestingly, the ribbonlike agglomerates appear as a relatively common form of aggregation for hairy-rod polyfluorene polymers. In the solid state, PF8 can form 2 nm thick ribbons reaching over hundreds of nanometers on surfaces.[66] PF2/6

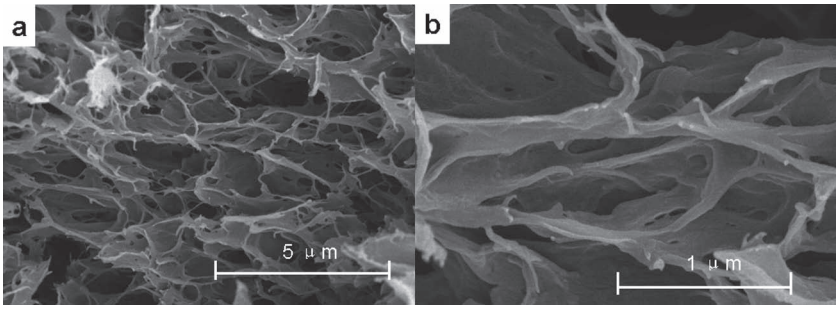

Figure 11. SEM images showing microporosity of PF8/DCE gel prepared by freeze-drying process. Reproduced with permission.[68] Copyright 2011, the American Chemical Society.

can form thicker, 20 nm thick ribbons also reaching over submicron distances.[67]

3.7. Microporous and Xerogel Structures

The structural hierarchy in polyfluorene gels is not limited to the submicron level. Lin et al.[68] worked on the gel consisting of PF8 in 1,2-dichlororoethane (DCE).[68] Akin to PF8/MCH, this material forms a gel based on a physical PF8 network with β-phase rich nodes. In this case the nodes are primarily cylindrical with stacked beta sheets inside the cylinders. Moreover, the authors introduce a new PF8 structure–xerogel which is a solid prepared from a PF8/DCE gel by freeze-drying. **Figure 11** shows SEM images of dried PF8 xerogel. The pore size is 2–5 μm which exceeds the dimensions in the abovementioned polyfluorene agglomerates.

4. Kinetics and Thermodynamics of Polyfluorene Solutions and Gels

4.1. Thermodynamics and Thermal Evaluation

The phase behaviors of both dilute, nominally dissolved polyfluorenes and dense aggregated polyfluorenes are supposedly temperature dependent. When polyfluorenes are nominally dissolved, i.e., when $c<c^*$, their main chain stiffness is influenced by temperature. In toluene, the persistence length of PF8 increases from 9.8 nm to 33.5 nm, when the temperature is raised from 25 °C to 50 °C.[60] Moreover, their side chain conformation and rotational freedom of repeat units are presumably influenced by temperature, this effect arising from the different interactions between solvent and side chain and between solvent and main chain as described by Dias, Vanden Bout and others.[55,69]

When the system is dilute, i..e. when $c<c^*$, cooling of polyfluorene mixtures is proposed to lead to the β-phase in two different ways. Dias et al.[55] conducted a systematic thermodynamic study for dilute PF8/MCH and described a two-step process when the temperature was dropped from room temperature to –13 °C. The first step is essentially a combined inter and intra molecular crystalisation (interdigitation) of the alkyl-chains from (rotationally) disordered α-conformation to the rotationally ordered β-conformation. These states may be understood to correspond to the C_α and C_β conformers of individual molecules.[33] While the interpretation of molecular details may differ from author to author, this step is presumably reversible and a response of changes in the quality of the solvent with temperature. The second step is the aggregation of the chains which contain β-conformers into anisotropic ordered domains. This state is intermolecular of its origin resembles the sheetlike β-aggregates found in higher concentrations, i.e., when $c>c^*$.[56]

The authors determined the transition equilibrium constant K_β

$$\ln K_\beta = \frac{\Delta S_\beta}{R} - \frac{\Delta H_\beta}{RT}, \quad (1)$$

using the temperature dependence of the 437-438 nm peak intensity and found the standard enthalpy ΔH_β = –18.0 kcal/mol and the standard entropy S_β = -68.4 kcal/mol. This finding illustrates that the β-phase formation is an exothermic process and involves a considerable entropy loss. The controlling factors are the interaction between the chains on adjacent monomers, the interaction between alkyl chains and the polymer backbone and the ordering (planarization) of the backbone conformation. In this picture, it is not possible to say whether PF8 polymers are completely isolated in the first step but emission and absorption spectra indicate that they do not involve intermolecular interactions between polymer backbones.

Alternatively, the individual PF8 chains in dilute MCH solution may form compact clusters where polymer-polymer interactions within the individual chain lead to the main chain planarization and optical fingerprint of β-phase as proposed by Vanden Bout and co-workers.[69] This picture may not necessarily explain the β-phase which is found for PF8 that contains only 13 repeat units, thus having the overall length ~10.5 nm which corresponds to the polymer persistence length, ~10 nm.

This initiation of β-phase in dilute systems is illustrated in **Figure 12** which plots the absorption spectra of PF8 in dilute 3 μm/mL MCH with decreasing temperature once the mixture has been anealed at 90 °C.[55] The data shows a growing peak at 437 nm appearing at –3 °C. This is the optical signature of β-phase. The appearance of this peak is connected to an isobestic point at 399 nm indicating equilibrium between two absorbing entities and an A→B type reaction from non-beta segments to beta-segments. This effect is reversible and the signature disappears but with strong hysteresis, after reheating up to 90 °C.

When the system is dense, i.e., when $c>c^*$, PF8 tends to aggregate in MCH upon cooling, and both the optical and crystallographic signatures of β-phase are obtained and the material is gelated. This means that strong intermolecular interactions are able to planarize polymer backbone leading also to domains of 3-dimensional chlathrate structure, likening to the solid state β-phase, within the mixture. Most notably, the aggregation tendency holds for the aggregate types (see Section 3.5.) regardless of their β-phase content. **Figure 13** plots the scattering intensities of PF8/MCH with increasing temperature.[65] This gives the

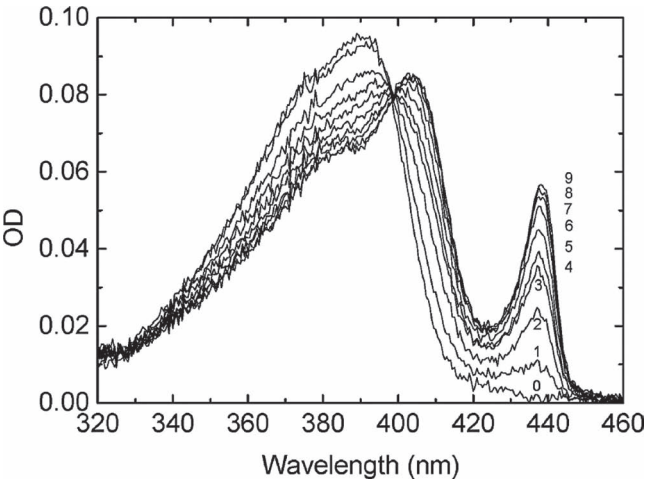

Figure 12. Growth of an absorption band below the π–π* transition in dilute PF8 cooled from 22 °C (1) to –144 °C (9) in MCH. Reproduced with permission.[55] Copyright 2006, the American Chemical Society.

fraction estimation for loose membranes and locally isolated chains based on the small-angle X-ray scattering (SAX). The β-phase is located in the crystallites within the membranes and distinguished from the loose membranes by a Bragg reflection. Like the aggregation tendency, the transition from the sheetlike structures to the isotropic phase occurs somewhat below 80 °C marked by the dashed vertical lines.

4.2. Kinetics and Time Evaluation

The polyfluorene aggregation in MCH develops in hours and days. **Figure 14** shows the time evaluation of the absorption

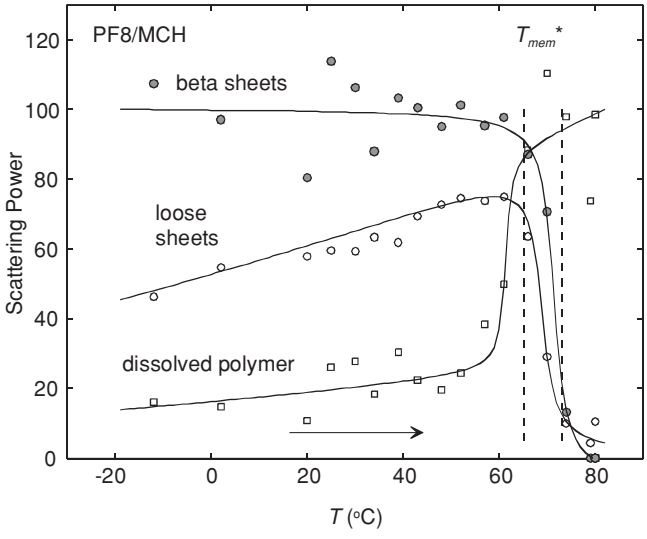

Figure 13. Scattering intensities as a function of temperature. The scattering components related to the weakly ordered β-sheets (solid circles), loose sheetlike membranes (open circles) and dissolved rodlike polymers (open squares) in a 10 mg/mL PF8/MCH. The order-disorder transition T^*_{mem} is marked by vertical dotted lines. Reproduced with permission.[64] Copyright 2008, the American Physical Society.

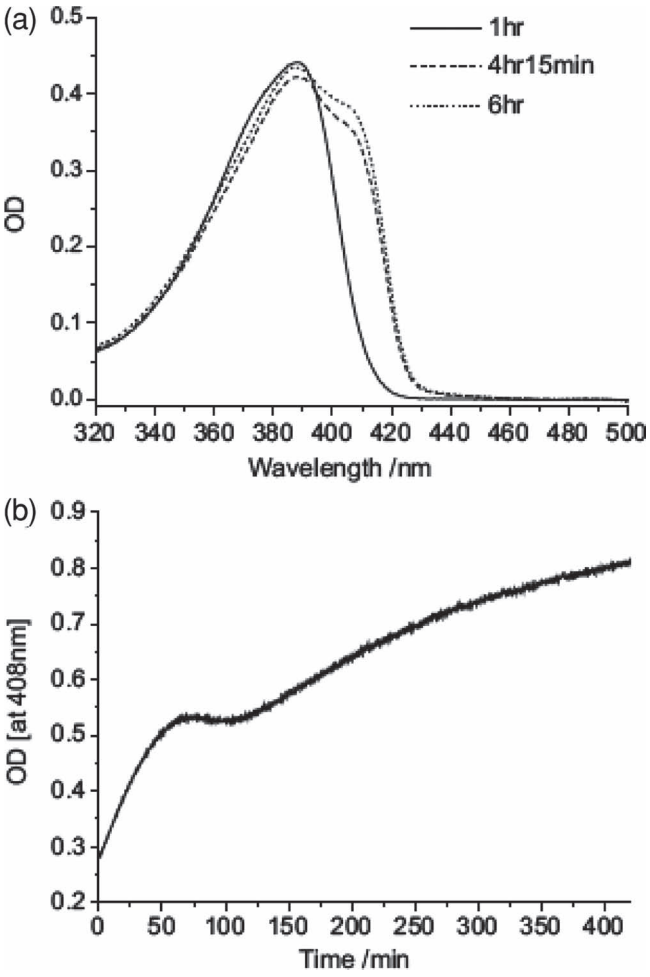

Figure 14. (a) The absorption spectrum of 6 µg/mL PF6/MCH, taken at intervals after boiling the solution and then returning to 295 K. (b) The absorption at 408 nm of stirred 20 µg/mL solution of PF6/MCH against time. Reproduced with permission.[62]

data of dilute PF6/MCH when the polymer is dissolved at the boiling point of MCH, 101 °C. The mixture is dilute, that is to say the concentration is below the overlapping concentration c^*. Initially the data show no signs of polymer associations but within a few hours the spectra shift and becomes structured indicating aggregation. However, this is not a sign of β-phase as described for PF8.

Figure 15 shows the time evaluation of SANS data of semidilute PF6 in toluene at room temperature after heating at 84 °C. PF6 dissolves better in toluene than MCH and in this case the system is dence, i.e. $c > c^*$. Following the trend in optical data, the PF6 chains appear first as locally isolated single chains but a sign of sheetlike aggregates is seen at 1 hour. The fraction of aggregates becomes higher with time and the aggregates become larger such that their thickness grows from 1 to 9 nm in 10 days. PF8 is not a gel at room temperature in toluene but aging dense toluene solutions at –20 °C for 24 hour leads to both gelation and appearance of β-phase.[60] When this system

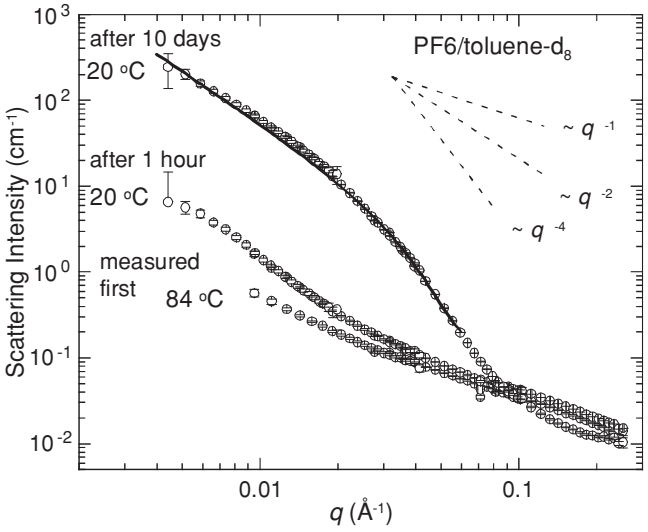

Figure 15. SANS data of PF6/toluene-d_8 measured at 84 °C as well as at 20 °C 1 hour and 10 days after heating. The solid line plots the fit to the sheetlike model. Reproduced with permission.[95] Copyright 2008, Elsevier.

is heated, an isotropic phase is reached at lower temperatures for toluene than for MCH, namely at 45 °C compared to 80 °C.

Dias et al.[55] conducted a systematic kinetic study for dilute ($c<c^*$) PF8/MCH and described the abovementioned two-step process when the temperature was dropped from room temperature to −13 °C. In this process, PF8 may form β-segments within the dissolved chains, these segments differing from the rest of polymer in terms of main chain planarity, followed by an aggregation.[55] The optical fingerprint of β-phase emerged when the temperature was dropped from room temperature to −13 °C and this process saturated in about 3 hours. The authors illustrated these steps using the equations

$$\alpha \underset{k_1}{\overset{k_{-1}}{\rightleftarrows}} \beta, \tag{2}$$

which describes the formation of β-conformers within a PF8 chain and

$$\beta_1 + \beta_k \underset{k_{diss}}{\overset{k_{agg}}{\rightleftarrows}} \beta_{k+1}, \tag{3}$$

which describes the aggregation of β-conformers. The rate constants represent direct and reverse reactions and β_k refers to an aggregate formed by k ordered β-domains. The authors determined the rate constants at −13 °C and found $k_{\alpha\rightarrow\beta} = 5.9 \times 10^{-4}$ s^{-1} and $k_{\beta} \rightarrow \alpha = 9 \times 10^{-4}$ s^{-1} for the first intramolecular step and $k_{agg} = 2.3 \times 10^{-3}$ s^{-1} and $k_{diss} = 2.3 \times 10^{-3}$ s^{-1} for the aggregation step. The values are relatively small and explain hours long times required for a complete β-phase conversion.

Chen et al.[70] conducted a systematic aging study for dense ($c>c^*$) PF8/MCH and concluded that the interconnected structure of PF8 rich domains is formed via spinodal decomposition mechanism (SD). This means that PF8/MCH mixture is homogeneous but not stable at the beginning of aging process and that the final morphology is driven by an eventual macrophase separation. **Figure 16**a shows how the light scattering intensity of PF8/MCH develops in 10 days time.[70] The intensity remains essentially constant within the first 3 hours (region I) after which it increases exponentially for the next 8 hours (region II). The semilog plot in the inset shows that the time dependence of the scattering intensity in the region II follows the exponential relationship prescribed by the Cahn-Hilliard model. Subsequent saturation in the region III stems from the coarsening effect of SD. Figure 16b shows a polarized optical micrograph of aged gel illustrating liquid crystalline (i.e. sheet containing) domains and isotropic liquid, this situation corresponding to the schematics in Figure 10b.

The time evaluation of β-phase in solutions and gels should be compared to the time evaluation of β-phase in thin films. Winokur et al.[43] studied PF8 films drop cast from THF and toluene as a function of time and approached the ODT on both cooling and heating. Elsewhere, Caruso and Anni[71] followed the vapour swelling and subsequent transition from glassy phase to the β-phase in real time at room temperature. Both groups shown that the fraction of β-phase follows the Avrami type expression

$$f_\beta = 1 - \exp(-bt^n), \tag{4}$$

where b is the rate constant, t is the elapsed time and n is the exponent related to the nucleation type.

Winokur et al. found that the transition to the β-phase on cooling follows an exponent n~1 law, which indicates diffuse free 1D crystallization and the crystallization to the "beta crystals". This process requires molecular-level conformational relaxation. In contrast, Caruso and Anni found n~0.5 for toluene and iso-octane and concluded that this corresponds to the athermal (simultaneous) nucleation followed by a diffusion controlled growth of 1D fibrillar beta crystals. This process thus differs from observed for the β-phase in thermal cycling. Winokur et al. found that thinner films have faster kinetics than thicker ones. Similarly, Caruso and Anni shown that the transition solvent induced swelling being much faster (4-12 minutes) in films than reported for elsewhere for solutions. Contrary to the results of Dias and others the fastest transition was reported for relatively good solvent toluene while the nonsolvent *n*-butylic alcohol did not lead to the β-phase at all.

5. Molecular Parameters to Control Structure and Photophysical Properties in Polyfluorene Solutions and Gels

5.1. Solvent and Polymer Concentration

Solvent matrix and polymer concentration control the structure and photophysics of polyfluorene mixtures. For PF8, the tendency to aggregation, gel and β-phase formation are driven by poorer solvents. The formation of β-phase is essentially independent on concentration if the concentration range is within the same order of magnitude, say 3–25 μg/mL MCH[55] or 1–10 mg/mL toluene.[56] However the aggregation and gelation tendencies are strengthened if the concentration is increased

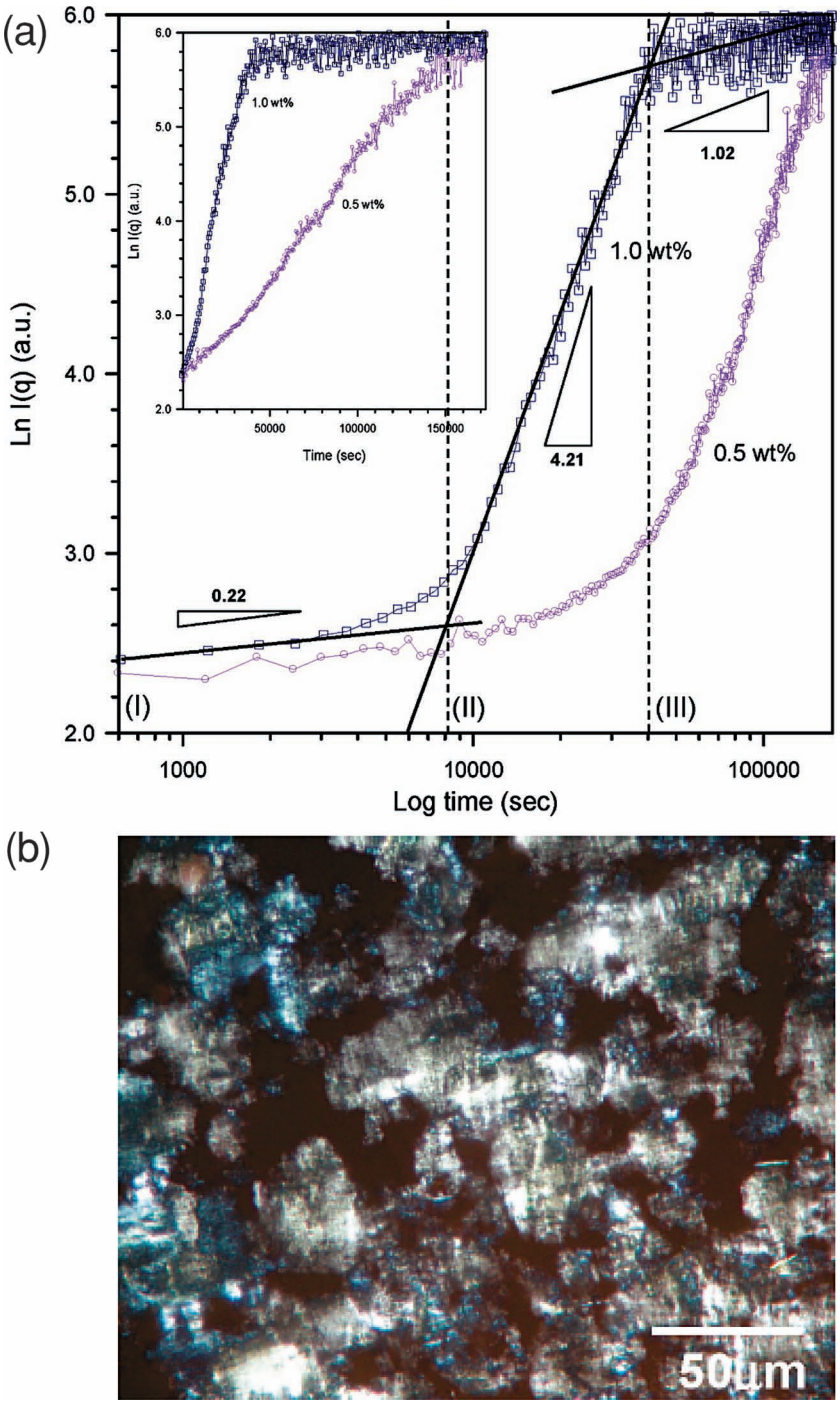

Figure 16. (a) The light scattering intensity during the aging of 0.5 and 1.0 wt% PF8/MCH mixtures at 20 °C illustrating three regions for the 1.0 wt% solution. (b) A polarized optical micrograph taken after 33 hours aging to demonstrate the interconnection of the liquid crystalline domains (of sheetlike structures) after the phase separation. Reproduced with permission from.[70] Copyright 2010, the American Chemical Society.

many orders of magnitudes, presumably if the concentration c is increased from $c<c^*$ to $c>c^*$. **Figure 17** shows our SANS data of PF8 in deuterated toluene and deuterated MCH. The curves are totally different with the slopes –1 and –2. This means that PF8/toluene is dominated by stiff, locally separated polymer sections, whereas PF8/MCH is dominated by sheetlike structures.[56] Simultaneously, strong optically observed β-phase contribution follows the observed sheets.

Kitts and Vandenbout[72] studied the β-phase fraction in various 1% mixtures upon a +60 °C and –78 °C heating cooling cycle and found the β-phase fraction increased in the series chloroform, toluene, cyclohexane and tetrahydrofurane. The gelation was observed for the last 3 mixtures but not in the best solvent, chloroform. Similarly, the transition temperatures from isotropic to gel (–55 °C, –25 °C and 10 °C) and gel to isotropic (53 °C, 50 °C and 73 °C) increased when the better solvent was replaced by a poorer one.

An interesting way to control the β-phase was described by Huang et al.[73] These authors studied PF8 in trinary chloroform/ethanol mixture and found a phase boundary from "mesoscopic" to "macroscopic" aggregates between 30% and 40% ethanol content such that the β-phase content increased to this boundary and saturated after it. This behaviour is essentially similar to the toluene/MCH pair. Moreover, the authors took a sample below the found phase boundary (i.e. when the ethanol content is less than 30%) and followed its behaviour in terms of a desolvation experiment by gradually removing the solvent mixture. This lead to the increase of the β-phase fraction associated with the increase of aggregate size with increasing polymer concentration. When this experiment was repeated above the phase boundary (i.e. when the ethanol fraction was more than 40%) this fraction remained largely constant. These concepts are not limited to the homopolymers. In recent work high β-phase content has been reported for example for PF8 copolymer with Iridium (III) complex in trinary THF/water solvent/nonsolvent mixtures.[74]

5.2. Side Chain Length

5.2.1. Optical Trace of β-Phase

Bright et al.[62] used optical spectroscopy and studied linear side chain polyfluorenes in dilute MCH as a function of side chain length, N. The sample concentration was ~7 μg/mL and each sample was treated by a heating cooling cycle (up to 100 °C and down to minus 51 °C) prior measurements. The authors observed a nonlinear relation between the β-phase fraction and the side chain length such that the optical signature of β-phase was seen for PF7, PF8 and PF9 at room temperature[62] and for PF10 at lower

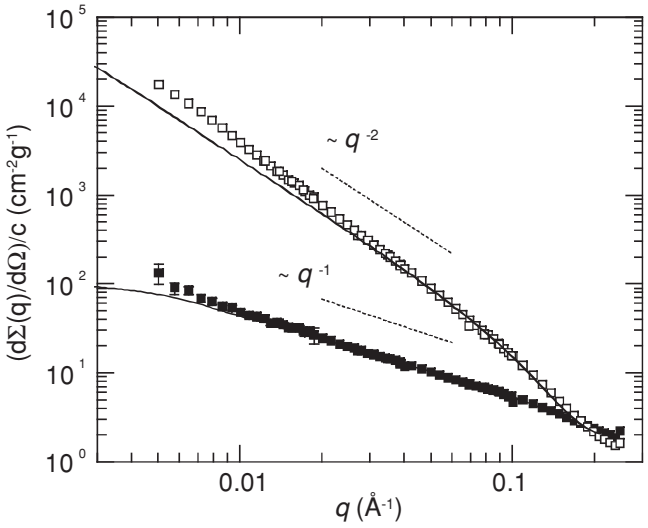

Figure 17. SANS data of PF8 in toluene-d_8 (solid squares) and MCH-d_{14} (open squares) when the concentration was 10 mg/mL. Reproduced with permission.[56] Copyright 2006, the American Chemical Society.

temperatures,[75] this signature being strongest for PF8. This dependence was attributed to a balance between two factors. The first factor is the dimer/aggregate formation, which is poorer for longer (more disordered) side chains. The second is the strength of Van der Waals interactions (between the side chains and backbone) to overcome the steric repulsion and planarize the backbone, which is insufficient for PF6. This study shows how the β-phase formation is strongly dependent on the side chain length. These results were deduced from the samples whose concentration ~7 μg/mL obeys $c<c^*$ condition but when the authors diluted the samples down to the ultralow concentration ~10 ng/mL, they observed reversible β-phase formation after similar thermal cycling. They expected that this β-phase originates from the well dispersed aggregates which were already present in more concentrated solutions before dilution.

Figure 18 plots the area normalized optical densities for the same systems at room temperature after identical thermal treatment but with 1000 times higher polymer concentration, 10 mg/mL, the mixture thus obeying $c>c^*$ condition. Also shown are model fits to the prominent spectral components and asymmetric β-peak. The β-phase is observed for PF8 and PF9, and marginally for PF10.[65] In another study the β-phase was optically observed in similar conditions also for PF7[61] so in this respect the high and low concentration systems are essentially similar.

Unlike the low concentration samples, the high concentration samples appear as gels at room temperature apart from liquid like PF10/MCH. The Huang-Rhys factors for the main spectral components change strongly with increasing N and these components can be associated with the above described structural levels in the gel.[65] The first vibronic feature, $v1$ is attributed to the locally free chains without intermolecular contacts while $v2$ and $v3$ are associated with the loose (non-beta) membranes and ordered (non-beta) sheets. The $v2$ peak increases at the expense of the $v3$ peak with increasing N, thus pointing to the increasing lateral freedoms within the sheets with increasing N. This means that the motion along the long

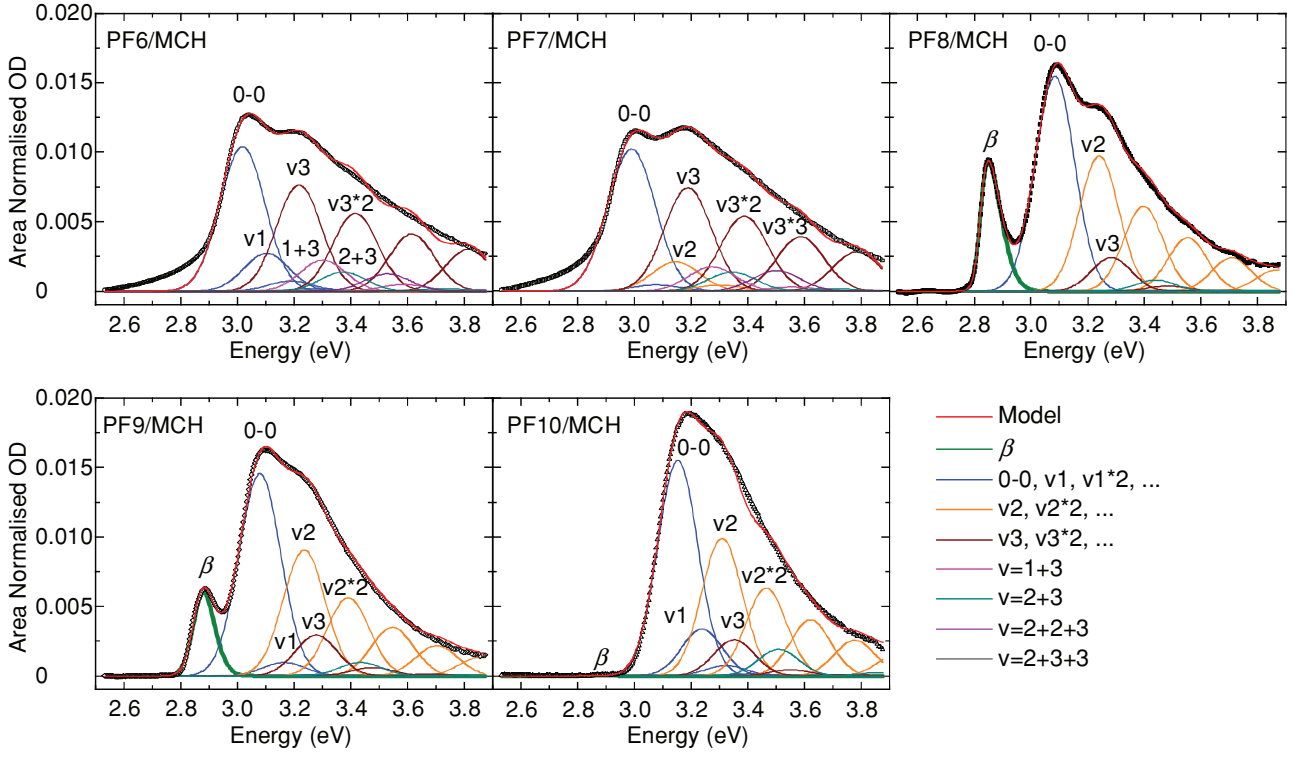

Figure 18. Area normalized optical density for linear side chain PFs in dense MCH gels after a heating cooling cycle, fitted with vibronic replicas and overtones. Reproduced with permission.[65] Copyright 2011, the American Physical Society.

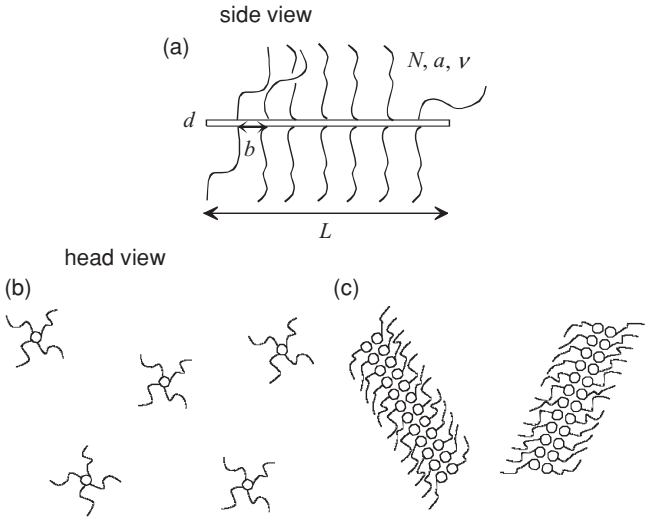

Figure 19. (a) A hairy-rod molecule. *N*, *a*, and *ν*, are, respectively, the number of side chain beads as well as its statistical length and excluded volume, while *b*, *d*, and *L* are, respectively, the grafting distance, diameter, and the length of the backbone. (b) Solution of non-interacting hairy-rods. (c) Solution of hairy-rod membranes. A simplified 2-dimensional picture is drawn with the rods parallel (a) or perpendicular (b and c) to the drawing plane. Reproduced with permission.[64] Copyright 2008, the American Physical Society.

chain axis is more restricted for $N = 6$ or 7 and the molecules have larger freedom to vibrate for $N \geq 8$. The loose membranes and the β-phase manifest weak order along *a*-axis (perpendicular to the sheet surface). The laterally restricted motion for $N = 6$ or 7 is consistent with the WAXS data which shows crystalline order along *b*-axis (perpendicular to the chain axes) for the ordered sheets of PF6 and PF7.[65]

5.2.2. Sheetlike Aggregates and Isotropic Phase

Figure 8 plots room temperature SANS data for PF6, PF7, PF8, PF9 and FP10 in 10 mg/mL MCH after a heating cooling cycle, these samples corresponding to ones whose optical data are shown in Figure 18. The SANS data indicate existence of submicron sized agglomerates being built by nanometer sized sheetlike entities for PF6-PF9; and the system of overlapping chains with segmental aligned nodes for PF10.[65] Thus, it is clear that the side chain length has a major influence on the polyfluorene phase behavior in MCH.

The polyfluorene phase behavior in dense mixtures has been predicted theoretically.[64] This approach interpretes polyfluorene as a hairy-rod molecule whose name comes from a rigid cylinder with flexible side chains attached to it (**Figure 19**a). The interaction between rigid backbone and solvent favors demixing (or macrophase separation). The hairy-rods can be dissolved to form a dilute solution of non-interacting molecules at high temperatures (Figure 19b) but they demix on cooling. Furthermore, sheetlike intermediate structures denoted membranes (Figure 19c) can appear on the way from the isotropic solution to the demixed state. The membrane term is justified[64] since these structures can be theoretically considered as bilayers and since this is experimentally supported in terms of sheet thickness.

Ref. [64] considered the scaling behavior of the solution-membrane transition temperature as a function of the side chains length by comparing the free energies of both phases. The free energy of the isotropic solution phase reads as

$$F^{(sol)} = F^{(sol)}_{brush} + F^{(sol)}_{RS} + F^{(sol)}_{RA} + F^{(sol)}_{tr}, \tag{5}$$

where the brush term $F^{(sol)}{}_{brush}$ includes the excluded volume interaction between the alkyl chains in a good solvent and their stretch which has been calculated.[76] Per side chain this contribution reads as

$$F^{(sol)}_1 = k_B T \left(\frac{\nu N}{a^2 b}\right)^{1/2}, \tag{6}$$

where ν is the excluded volume of a side chain monomer in a good solvent, *N* and *a* the number of side chain beads (units per side chain) and its statistical segment length, respectively, and *b* the grafting distance along the backbone (Figure 19a). Terms $F^{(sol)}{}_{RS}$ and $F^{(sol)}{}_{RA}$ represent the interaction of the backbone rod "R" with solvent "S" molecules and alkyl chains "A", respectively. Term $F^{(sol)}{}_{tr}$ incorporates the translational free-energy of the hairy-rod molecules.

The rod-solvent interaction free energy is estimated as

$$\frac{F^{(sol)}_{RS}}{N_{tot}} = 2Ld\gamma_{RS}\nu_0 c^{(sol)_2}, \tag{7}$$

following the methods described by Stepanyan et al.[77]. Here the "interfacial" energy parameter γ_{RS} describes the interaction between backbone and solvent. *L* and *d* are the length and the diameter of the stiff backbone, N_{tot} is the total number of molecules in the system, ν_0 the monomeric volume, and $c^{(sol)}{}_2$ the concentration of the solvent molecules in the vicinity of the backbone (see Figure 19a).

Using the same arguments, the free energy for the rod-alkyl chain interaction is estimated as

$$\frac{F^{(sol)}_{RA}}{N_{tot}} = 2Ld\gamma_{RA}\nu_0 c_2, \tag{8}$$

where c_2 is the concentration of the alkyl monomers around the backbone such that $\nu_0(c^{(sol)}{}_2 + c_2) \equiv 1$.

The last term in the Equation (5) describes the translational entropy as

$$F^{(sol)}_{tr} = k_B T N_{tot}\left[\ln\frac{f}{e} + \frac{1-f}{\nu_0 f}\left(\frac{\pi d^2 L}{4} + \frac{\nu_0 NL}{b}\right)\ln\frac{1-f}{e}\right], \tag{9}$$

where *f* is the volume fraction of the polymer in the system.

Finally, the free energy of the isotropic solution phase in Equation (5) takes the form

$$\frac{F^{(sol)}}{N_{tot}k_B T} = \frac{L}{b}\left(\frac{\nu N}{a^2 b}\right)^{1/2} + 2Ld\left[\frac{\gamma_{RS}}{k_B T}(1-\nu_0 c_2) + \frac{\gamma_{RA}}{k_B T}\nu_0 c_2\right] + \ln\frac{f}{e} + \frac{1-f}{\nu_0 f}\left(\frac{\pi d^2 L}{4} + \frac{\nu_0 NL}{b}\right)\ln\frac{1-f}{e}, \tag{10}$$

with $c_2 = \left(a^2 b^2 d^2 \nu\right)^{-1/3}$ calculated based on the formulas given in Subbotin et al.[76]

The free energy of other competing phase, the solution with membranes, can be calculated using same ideas which yield

$$\frac{F^{(mem)}}{N_{tot} k_B T} = \frac{2NL}{b}\left(\frac{\nu}{abd}\right)^{2/3} + Ld\left[\frac{\gamma_{RS}}{k_B T}\left(1-\nu_0 c_1\right) + \frac{\gamma_{RA}}{k_B T}\nu_0 c_1\right] + \frac{1-f}{v_0 f}\left(\frac{\pi d^2 L}{4} + \frac{\nu_0 NL}{b}\right)\ln\frac{1-f}{e}, \quad (11)$$

where $c_1 = \nu^{-1/3}(abd)^{-2/3}$ is the concentration of the alkyl monomers around the backbone bilayers. $F_1^{(mem)} = 2N(\nu/(abd))^{2/3}$ stands for the planar brush free energy per chain.[78] The interaction free energy is corrected by the fact that only a half of the surface area of the rods is in contact with the solvent or side chains.

When equations Eqs. (10) and (11) are equated, this lead to an estimation of the membranes-isotropic solution transition temperature, T_{mem}*, as

$$\frac{1}{k_B T_{mem}*} = \frac{2(\nu/abd)^{2/3} N - \left(\nu/a^2 b\right)^{1/2}\sqrt{N} - (b/L)\ln(f/e)}{bd\left[\gamma_{RS} + (\gamma_{RA}-\gamma_{RS})\nu_0(2c_2 - c_1)\right]} \quad (12)$$

Here it has been assumed that ν, γ_{RA}, and γ_{RS} do not depend on the temperature. This assumption is generally incorrect but it does not change the scaling behavior of T_{mem}*.

The Equation (8) is valid for relatively long side chains, at least so long that the distance between their grafting points is smaller than their Flory radius $R_F = a\left(\nu/a^3\right)^{1/5} N^{3/5}$, i.e., $N > N^* = (b/a)^{5/3}\left(\nu/a^3\right)^{1/3}$. For shorter side chains and essentially rodlike polymers we can expect a picture where isotropic liquid demixes with decreasing temperature.[17]

The polymer-solvent demixing was addressed through an approach where long enough side chains demix into a highly concentrated, almost a melt, phase (with sheetlike morphology) and virtually pure solvent. This idea has a strong experimental support.

The free energy after demixing is of the order of

$$\frac{F^{(demix)}}{N_{tot} k_B T} = \frac{3NL}{2b}\left(\frac{\nu}{abd}\right)^2 + Ld\frac{\gamma_{RA}}{k_B T}, \quad (13)$$

where $F_1^{(lam)} = 3/2 k_B T N(\nu_0/(abd))^2$ is the elastic energy per side chain following the details shown by Stepanyan et al.[77]. The free energy of demixing, Equation (13), scales in a similar fashion to that of the membrane phase, Equation (11), which implies that either the regime of thermodynamic stability of membranes is narrow or the membranes are thermodynamically unstable. Accordingly, the demixing temperature, T_{IN}* becomes

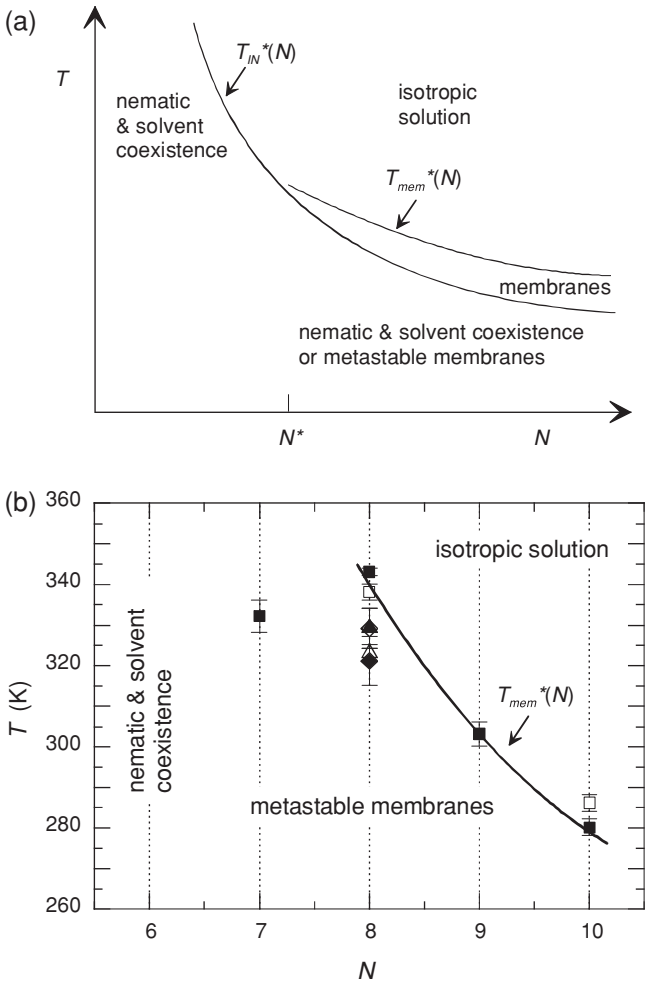

Figure 20. (a) Theoretical presentation of transition temperatures $T*_{IN}(N)$ and $T*_{mem}(N)$ as a function of side chain length *N*. (b) Experimental presentation of the transition temperature $T*_{mem}$ as a function of *N* for linear side chain polyfluorenes in MCH. The experimental data are based on SAXS (solid squares) and DSC (open squares) measurements. Also shown are corresponding transition for PF2/6-F8 copolymers where the ratio of F2/6 units to F8 units is 95:5 (triangles) and 90:10 (diamonds) derived from the SAXS (solid symbols) and DSC (open symbols) measurements. Reproduced with permission.[64] Copyright 2008, the American Physical Society.

$$\frac{1}{k_B T_{IN}*} = \frac{\frac{3}{2}\left(\frac{\nu}{bad}\right)^2 N - \left(\frac{\nu}{a^2 b}\right)^{1/2}\sqrt{N} - \frac{b}{L}\left[\ln\frac{f}{e} + \frac{1-f}{v_0 f}\left(\frac{\pi d^2 L}{4} + \frac{\nu_0 NL}{b}\right)\ln\frac{1-f}{e}\right]}{bd\left[\gamma_{RS} + (\gamma_{RA}-\gamma_{RS})(1-\nu_0 c_2)\right]}, \quad (14)$$

and is expected to be close to the membranes-isotropic transition temperature, $T*_{mem}$.

Figure 20a plots the theoretical phase diagram for linear side hairy-rod polymers in a poor solution as a function of side chain length.[64] The theory predicts isotropic solution for high temperatures and for long side chains and nematic phase coexisting with the solvent or a possible metastable membranelike aggregates for low temperatures and short side chains. These phase regions are divided by a transition temperature $T*_{IN}(N)$,

where N is the number of side chain beads and which decreases with increasing N. Between these phases exist a narrow membranes phase, defined by transition temperature $T^*_{mem}(N)$ possible for side chain lengths higher than N^*, also decreasing with increasing N.

Figure 20b plots the experimental phase diagram for the linear side chain polyfluorenes in a poor solution MCH as a function of side chain length.[64] The theoretically predicted features are qualitatively found. When the side chain length is low, N^*~6, the material appears largely lyotropic without experimentally attainable isotropic phase. The sheets are tied together with a crystallite component. Above N^* both the isotropic and membrane phases exist, $T^*_{mem}(N)$ decreasing for N≥8. Notably PF10 forms sheetlike aggregates and shows a membrane-isotropic phase transition (between all sheetlike aggregates and an isotropic phase) at -5°C on heating.[64] The sheetlike aggregates are concomitant with the β-phase.[75] Interestingly, the experimental data shown in Figure 13 shows that the fraction of membranes is expected to *increase* just before they vanish at $T^*_{mem}(N)$ with increasing temperature, which is qualitatively consistent with the theoretically predicted idea of stable membranes just below $T^*_{mem}(N)$.

A peculiar feature not predicted by the above depicted theory is the odd-even effect in the average size of sheets.[61] The sheets for PF7 and PF9 appear thicker and laterally smaller than PF8 sheets and PF6 sheets. This information is seen in the shape of small-angle scattering curve as well as a broad interference maximum at 0.1-0.3 $Å^{-1}$ seen usually for PF7 and PF9 but not for PF8 (see a letter c in Figure 8). Conspicuously, this feature appears at the low scattering angle and is not any of the peaks seen for crystalline nodes in the WAXS data (Figure 7).

5.2.3. Agglomerates of Sheetlike Aggregates

The side chain length influences, moreover, the compactness of ribbonlike aggregates of sheets.[65]. This phenomenon is interpreted such that the probability for physical crosslinks between the moieties in a polyfluorene gel increases with decreasing N. At room temperature, this leads to the compact PF6 agglomerates and largely one-dimensional PF9 ribbons. **Figure 21** shows the outlined phase equilibria of ribbonlike agglomerates of polyfluorene sheets in MCH against the side chain length. The interaction between the ribbons and solvent, represented by the parameter $\bar{\chi}$ depends on the sidechain length (6-10). f is the limiting volume fraction of membranes. The biphasic region within the "cup" yields almost pure solvent on the right and the solution of the ribbons on the left from the minimum. The arrow shows that the polymer concentration in the ribbon-rich domains is expected to grow with increasing N. When the temperature is constant (room temperature in our case), no phase separation occurs at certain side chain length (N = 10).[65]

5.3. Side Chain Branching

Linear side chain PF8 shows sheetlike aggregates in MCH as illustrated in Figure 10. In a sharp contrast, the branched side chain PF2/6 manifests a system of locally isolated rigid chains which will overlap when $c>c^*$.[64] Furthermore, even though PF2/6 shows a sign for aggregation at –20 °C in 5-50 mg/mL

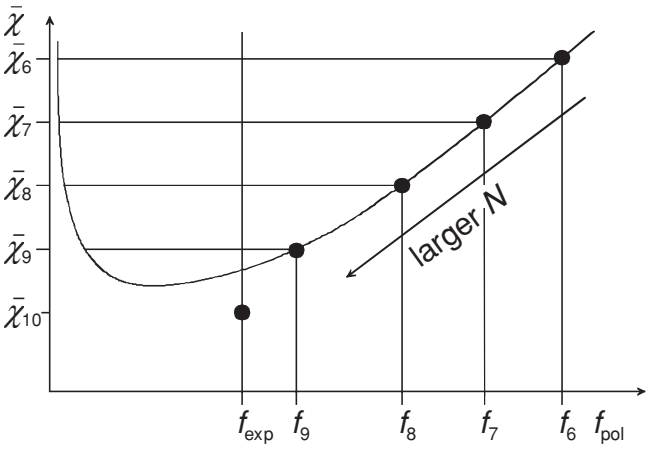

Figure 21. Illustration of the phase equilibria in the ribbonlike agglomerates of polyfluorenes in MCH. $\bar{\chi}$ is the effective interaction parameter between the ribbons and solvent and f is the limiting volume fraction of membranes. Reproduced with permission.[65] Copyright 2011, the American Physical Society

toluene[79] the β-phase is never reported for it. An apparent question is where in between there is a transition from one behaviour to another. Random copolymers consisting of F2/6 and F8 units were originally introduced by Scherf, Winokur and coworkers[80] and these materials allowed us to screen the nature of polyfluorene/MCH mixtures as a function F2/6 content, thus essentially as a function of side chain branching.[81]

Figure 22 plots optical absorption curves for branched side chain PF2/6, linear side chain PF8 and selected F2/6-F8 random copolymers in MCH after a heating cooling cycle. The signature of β-phase is visible when the F2/6 fraction is 5 or 10% but not when the fraction is raised up to 50%. This signature is concomitant with the with sheetlike aggregates[64] but the increasing F2/6 fraction decreases the transition temperature T_{mem}* as shown in Figure 20b.

Elsewhere, Bright et al.[82] began with PF8 and synthesized diverse copolymers by incorporating 8-20% dibenzothiophene (DBT) or 2–15% dibenzothiophene-*S,S*-dioxides (S-units) into PF8 polymer and studied these materials in toluene vapor treated films. The authors found the optical fingerprint of the β-phase, this fingerprint decreasing with the increasing DBT content to a 20% cutoff or with the inreasing S-unit content to a 12% cutoff. This is another example where PF8 backbone with copolymerizing units can be employed to control the fraction of beta emission sites.

5.4. Molecular Weight and Use of Oligomers

Vanden Bout and coworkers studied PF8 in MCH and varied molecular weight from 2.5 to 100 kg/mol corresponding to 5 to 216 monomer units.[69] The solution was so dilute (0.001 wt%) that the polymers justify the $c<c^*$ condition and cannot overlap if perfectly dissolved. They cooled these solutions down and expected that the PF8 polymer goes through the coil-globule

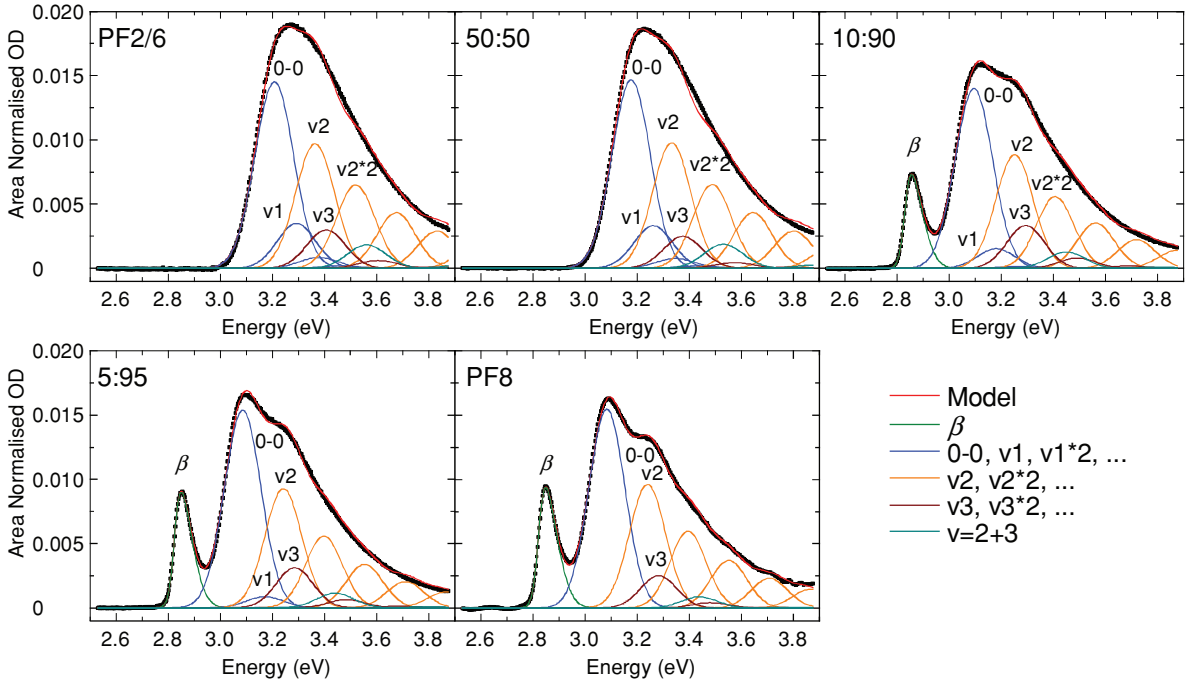

Figure 22. Area normalized optical density for PF2/6, PF2/6-F8 copolymers and PF8 in 10 mg/mL MCH. The numbers 50:50, 10:90, and 5:95 refer to the ratio of F2/6 units to F8 units. The solid lines are fits to different absorption components. Reproduced with permission.[81] Copyright 2011, the American Chemical Society.

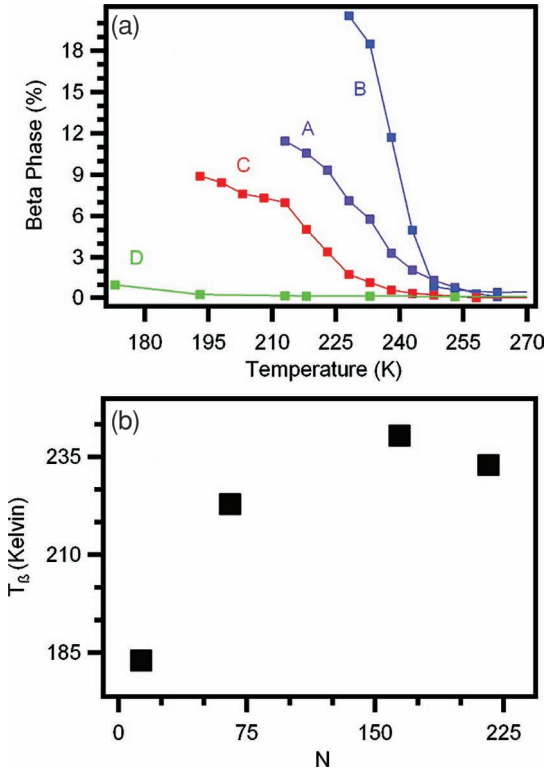

Figure 23. (a) The beta-phase content for four different PF8 batches in MCH during cooling. The numbers of monomer units were (A) 216, (B) 164, (C) 65 and (D) 13. (b) The observed transition temperature, T_β, as a function of molecular weight (main chain length), N. Reproduced with permission.[69] Copyright 2011, the American Chemical Society.

transition. The authors argued that when PF8 forms a compact globule the distinct parts of polymer interact and this leads to the main chain planarization and optical characteristics of β-phase. The higher the molecular weight, the higher this transition temperature was detected and the higher the β-phase fraction was found. The shortest polymer was plausibly too stiff for coiling, because its length was below the persistence length and it unsurprisingly showed no β-phase.

Figure 23 plots the β-phase content and transition temperatures as a function of molecular weight. Similar example where the transition from long to short and thus from flexible to rigid polyfluorene entities leads to a significant drop in the phase transition temperature has been known also for solid state PF2/6.[28]

In the solid state, polydisperse short PF2/6[28] behaves differently to the monodisperse F2/6 oligomers introduced by Wegner and coworkers.[31,38,39] While PF2/6 adopts a nematic phase, F2/6 oligomers remain crystalline. This difference has motivated diverse investigations of F2/6 oligomers in solutions. Somma et al. studied F2/6 oligomers in a good solvent toluene.[83] While PF2/6 polymers behave as wormlike chains in dilute toluene,[54] the authors found that the monodisperse F2/6 oligomers from trimer to heptamer[83] behave as rigid rod cylinders. The thickness of these cylinders is 0.6 nm and the length 0.75 nm times the number of oligomer repeat.

When the concentration is increased, the discussed oligomers begin to interact and show a lyotropic phase above the concentration c^*, which is found to be 600–900 mg/mL with decreasing oligomer length. When the concentration is increased up to 30 wt%, large spherical agglomerates form. The lyotropic phase corresponds to the aggregate phase of

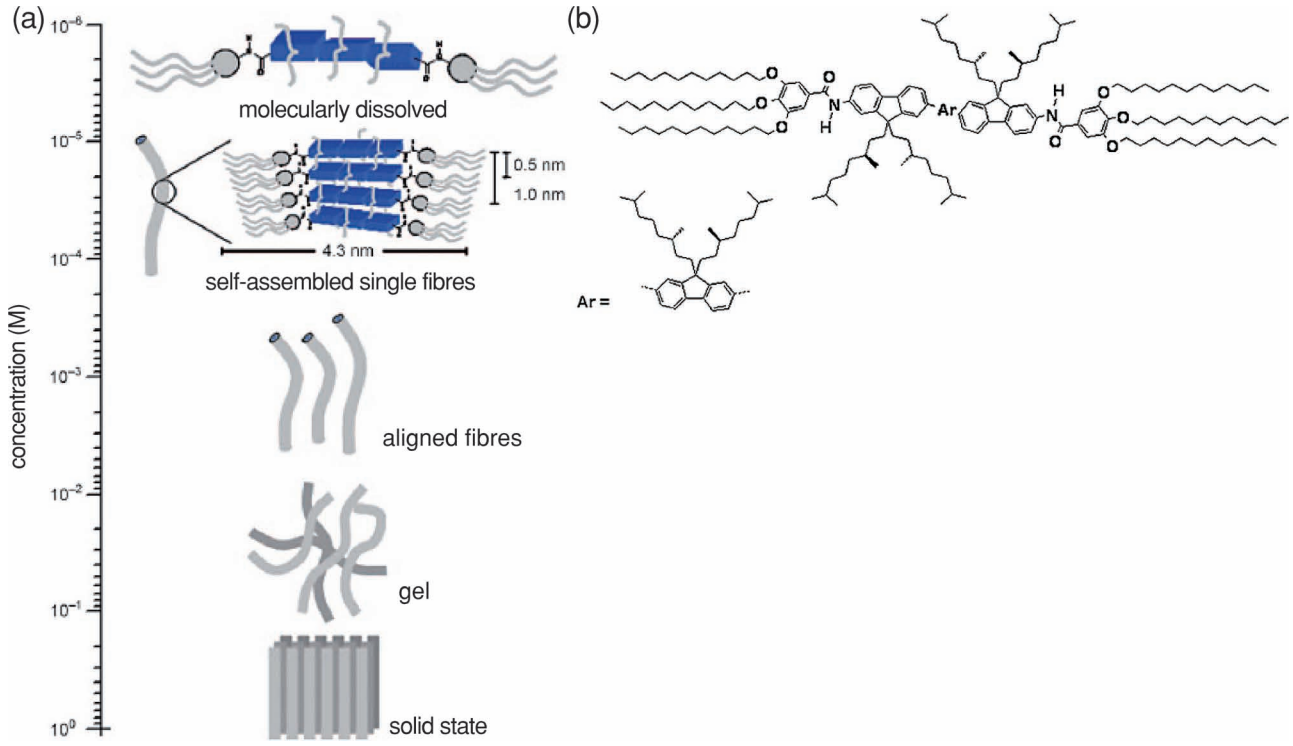

Figure 24. (a) Schematics of the concentration dependent phase behavior of a fluorene based co-oligomer in MCH at room temperature. (b) Chemical structure of the considered co-oligomer. Reproduced with permission.[84]

polyfluorenes but the spherical "micellar" agglomerates do not have their polymer counterpart. The formation of spheres may stem from the monodispersity of oligomers.

Abbel et al.[84] used advanced synthesis to prepare fluorene based oligomers and mixed them with MCH. The authors screened various oligomers and identified suitable chemical structure to avoid precipitation but leading instead to gelation; and tailored the energy transfer of this system allows white light emitting gels. This process is highly dependent on the oligomer concentrations. **Figure 24** illustrates structural steps of this material from solid state to the entangled gel of fibrous supramolecular structures, where oligomers are built perpendicular to the fiber axis, finally leading to the dissolved oligomers.

5.5. Small Molecule Additives

Above mentioned methods to control the structure and β-phase formation in polyfluorene mixtures are based on temperature or the chemical structure of polymer or solvent. In a few examples, an additional third compound influences the polymer structure. Deaggregation of π-stacking of poly(9,9-dihexylfluorene divinylene-alt-1,4-phenylenevinylene) has been demonstrated in clay nanocomposites by Tozoni et al.[85] Both constituents are soluble in toluene and polymer absorbs on the clay surfaces when the solutions are mixed. The additives can lead to the β-phase, as reported for PF8 when incorporated into the LC liposome bilayers.[86] Similarly, the β-phase is observed when ambipolar moieties are incorporated into the PF8 matrix.[87] Elsewhere, Bazan and coworkers[88] incorporated 1,8-dioctane into PF8 *o*-xylene solutions and used this as a β-phase promotor. In this system the β-phase content was varied between 0 and 45%, leading to rich morphological changes and even 50% increase in the efficiency of polymer LEDs.

5.6. Molecular Confinement

An intriguing possibility for the β-phase formation has been pioneered by Redmond and coworkers[89] involving a solution assisted template wetting. In this procedure, for example PF8 THF solution is incorporated into a porous alumina membrane under elevated pressure. PF8 constitutes a thin film which is soaked afterwards by aqueous NaOH. This leaves submicron sized tubular PF8 assemblies which are subsequently dispersed in poor solvent water by sonication. PF8 molecules are confined in the template and this confinement is not lost on the removal of template but - very prominently - leads to the uniaxial alignment and appearance of β-phase.

Fujiki and coworkers[90] dissolved a series of polyfluorenes into a dilute chloroform solution saturated with water and let the solvents evaporate on mica. While chloroform evaporates first the mixture becomes rich of water droplets. These droplets act as dynamic template leaving nano-sized and volcano shaped structures for PF6 and polymer rings for PF8 and PF10. In contrast, wormlike structures are observed for polyfluorenes with longer side chains, namely poly(9,9-didodecylfluorene) (PF12) and poly(9,9-ditetradecylfluorene) (PF14) and poly(9,9-dioctadecylfluorene) (PF18). PF10 evaporated from pure chloroform assembles

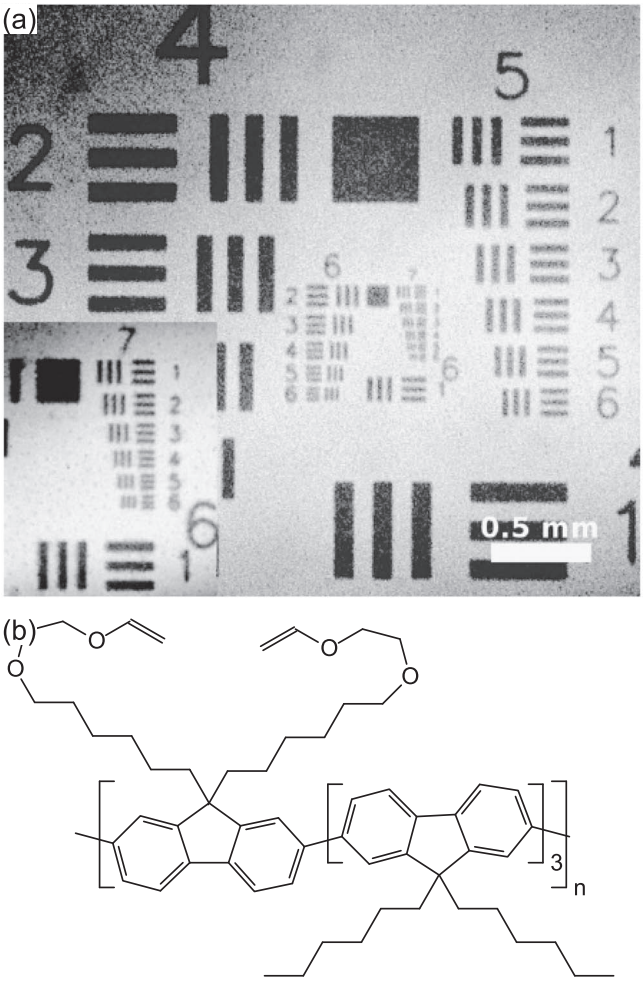

Figure 25. (a) Patterns of crosslinked vinyl ether functionalized PF6 (VE-PHF). (b) Chemical structure of VE-PHF. Reproduced with permission from.[93] Copyright 2011, Elsevier.

as nano-sized dots. Fujiki et al. observed β-phase optically for PF8 and PF10 rings but not for PF10 dots or other polyfluorenes.

Elsewhere, Evans and Marr introduced an ionogel where PF8 is incorporated into a silica matrix via sol-gel chemistry.[91] The interaction between this matrix and PF8 is based on the combination of hydrogen bonding and π-stacking and PF8 is confined and its backbone is planarized manifesting the photoluminescence of β-phase. This is a rare example of inorganic polyfluorene containing gels.

6. Permanently Cross-Linked Systems

While all the above mentioned examples concern physically cross-linked systems and physical gels we may expect apparent similarities amongst permanently cross-linked polyfluorenes. This kind of systems have been pioneered by Morgado and others[92] who synthesized fluorene based copolymers with reactive oxetane side groups and cross-linked this by UV-light. In this process they controlled solubility, a key factor from phase behavioural point of view. Elsewhere Kuehne et al.[52] functionalized PF8 and with vinyl ether groups. These authors induced the β-phase by toluene vapour and cross-linked and patterned this system by electron beam. Interestingly, this treatment did not suppress the β-phase and patterned structure allowed, moreover, optically pumped lasing. In another example, Kuehne et al.[93] functionalized PF6 with vinyl ether groups to form VE-PHF and cross-linked and patterned this material using UV-lithography. **Figure 25** shows a test pattern using this method. Interestingly, the VE-PHF polymer shows an aggregate phase when treated by *p*-xylene and this phase was not suppressed by cross-linking. The authors called this state a β-phase based on its closely related X-ray structure but this polymer does not exhibit an absorption shoulder which serves as the β-phase definition for PF8. Given the lack of the β-phase optical signature, it is more likely that this ordered phase is similar to that seen in PF6 but is not the β-phase.

7. Conclusions and Outlook

Within the solvent matrix, polyfluorene polymers can exist as individual, virtually isolated molecules and in nearly all possible structure types which manifest a complex hierarchy ranging from intramolecular and nanometer scale to the macroscopic scale finally approaching the solid state structures. The photophysical phenomena originate from the molecular and short-range intermolecular environment but they should be understood *vis-à-vis* the formation of larger length scale aggregates and agglomerates as these are manifestations from the molecular level factors. This picture in solvent matrices should also be mirrored to the known behaviour of isolated polymers and the solid state and to the corresponding phenomena seen in other π-conjugated polymers and hairy-rod polymers such as *p*-phenylene type polymers.

In this review we have illustrated perhaps the most important polyfluorene structures and relations between structure and optical properties in solutions and gels. We have presented coherent guidelines in terms of what parameters can control these processes and why they do so, in particular by using archetypical PF2/6 and PF8 polymers and their analogues and variants. The presented findings provide quantitative feedback for synthetic chemists in the search for more efficient chemical and molecular polyfluorene structures in solutions yet having implications in the organic electronics applications and solution processing in particular. Generalizations with the polyfluorenes with myriad functionalizations and well defined oligomers have already shown and external tools such as templates, surfactants and hybrid materials mimicking spatially arrested gel type structures as well as corresponding permanently cross-linked polymers with exiting properties are emerging. We expect that these trends will become increasingly active but the simultaneous fundamental structural and photophysical work continues to play a key role in the years to come.

Acknowledgements

When conducting this research line we have enjoyed collaboration with Prof. Ullrich Scherf of the University of Wuppertal, Dr. Fernando Dias and Dr. Daniel Bright of the University of Durham, Dr. Roman Stepanyan

of DSM Research, Dr. Mika Torkkeli of the University of Helsinki, Dr. Vasil Garamus of the Helmholtz-Zentrum Geesthacht, Dr. László Almásy of the Budapest Neutron Centre, Prof. Hugh Burrows of the University of Coimbra, Prof. Jorge Morgado of the Instituto de Telecomunicações and many others. We acknowledge funding from the European Commission.

Received: October 15, 2012
Published online: January 22, 2013

[1] K. Tashiro, K. Ono, Y. Minagawa, M. Kobayashi, T. Kawai, K. Yoshino, *J. Polym. Sci. B: Polym. Phys.* **1991**, *29*, 1223; M. J. Winokur, D. Spiegel, Y. Kim, S. Hotta, A. J. Heeger, *Synth. Met.* **1989**, *28*, C419.
[2] G. Perego, G. Lugli, U. Pedretti, M. Cesari, *Makrom. Chem.* **1988**, *189*, 2657.
[3] J. P. Pouget, M. E. Jozefowicz, A. J. Epstein, X. Tang, A. G. MacDiarmid, *Macromolecules* **1991**, *24*, 779; E. Banka, W. Luzny, *Synth. Met.* **1999**, *101*, 715; M. J. Winokur, B. R. Mattes, *Phys. Rev. B* **1996**, *54*, 12637.
[4] G. Mao, M. J. Winokur, F. E. Karasz, *Phys. Rev. B* **1996**, *53*, R463.
[5] M. Grell, D. D. C. Bradley, G. Ungar, J. Hill, K. S. Whitehead, *Macromolecules* **1999**, *32*, 5810.
[6] E. J. Samuelsen, A. P. Monkman, L. A. A. Pettersson, L. E. Horsburgh, K. E. Aasmundtveit, S. Ferrer, *Synth. Met.* **2001**, *124*, 393.
[7] L. H. Tremel, S. Uttiya, E. Crossland, S. Ludwigs, N. C. Vergnat, M. Brinkmann, *Adv. Funct. Mater.* **2011**, *21*, 4047; T. J. Prosa, J. Moulton, A. J. Heeger, M. J. Winokur, *Macromolecules* **1999**, *32*, 4000; M. L. Chabinyc, M. F. Toney, R. J. Kline, I. McCulloch, M. Heeney, *J. Am. Chem. Soc.* **2007**, *129*, 3226.
[8] G. Mao, M. J. Winokur, F. E. Karasz, *Phys. Rev. B* **1998**, *58*, 4089; M. J. Winokur, P. Wamsley, J. Moulton, P. Smith, A. J. Heeger, *Macromolecules* **1991**, *24*, 3812; M. Knaapila, R. Stepanyan, L. E. Horsburgh, A. P. Monkman, R. Serimaa, O. Ikkala, A. Subbotin, M. Torkkeli, G. ten Brinke, *J. Phys. Chem. B* **2003**, *107*, 14199.
[9] D. Gonzales-Rodriguez, A. P. H. J. Schenning, *Chem. Mater.* **2011**, *23*, 310.
[10] F. J. M. Hoeben, P. Jonkheijm, E. W. Meijer, A. P. H. J. Schennnig, *Chem. Rev.* **2005**, *105*, 1491; S. W. Thomas III, G. D. Joly, T. M. Swager, *Chem. Rev.* **2007**, *107*, 1339; A. J. Berresheim, M. Müller, K. Müllen, *Chem. Rev.* **1999**, *99*, 1747.
[11] G. Wegner, *Macrom. Chem. Phys.* **2003**, *204*, 347.
[12] M. Campoy-Quiles, T. Ferenczi, T. Agostinelli, P. G. Etchegoin, Y. Kim, T. D. Anthopoulos, P. N. Stavrinou, D. D. C. Bradley, J. Nelson, *Nature Mater.* **2008**, *7*, 158.
[13] H. Sirringhaus, P. J. Brown, R. H. Friend, M. M. Nielsen, K. Bechgaard, B. M. W. Langeveld-Voss, A. J. H. Spiering, R. A. J. Janssen, E. W. Meijer, P. Herwig, D. M. de Leeuw, *Nature* **1999**, *401*, 685; C. L. Donley, J. Zaumseil, J. W. Andreasen, M. M. Nielsen, H. Sirringhaus, R. H. Friend, J.-S. Kim, *J. Am. Chem. Soc.* **2005**, *127*, 12890; R. J. Kline, M. D. McGehee, M. F. Toney, *Nature Mater.* **2006**, *5*, 222.
[14] D. Vlassopoulos, G. Fytas, *Adv. Polym. Sci.* **2010**, *236*, 1; T. Kato, K. Tanabe, *Chem. Lett.* **2009**, *38*, 634.
[15] M. Shibayama, *Macrom. Chem. Phys.* **1998**, *199*, 1; S. Panyukov, Y. Rabin, *Phys. Rep.* **1996**, *269*, 1.
[16] G. Brodowski, A. Horvath, M. Ballauff, M. Rehahn, *Macromolecules* **1996**, *29*, 6962; G. Petekidis, D. Vlassopoulos, G. Fytas, N. Kountourakis, S. Kumar, *Macromolecules* **1997**, *30*, 919; G. Petekidis, D. Vlassopoulos, G. Fytas, R. Rülkens, G. Wegner, *Macromolecules* **1998**, *31*, 6128; G. Petekidis, D. Vlassopoulos, G. Fytas, R. Rülkens, G. Wegner, G. Fleischer, *Macromolecules* **1998**, *31*, 6139.
[17] M. Ballauff, *Macromolecules* **1986**, *19*, 1366.
[18] J. H. Burroughes, D. D. C. Bradley, A. R. Brown, R. N. Marks, K. Mackay, R. H. Friend, P. L. Burns, A. B. Holmes, *Nature* **1990**, *347*, 539.
[19] D. Perahia, R. Traiphol, U. H. F. Bunz, *J. Chem. Phys.* **2002**, *117*, 1827.
[20] D. Perahia, X. Jiao, R. Traiphol, *J. Polym. Sci. Part. B: Polym. Phys* **2004**, *42*, 3165.
[21] S. H. Chen, A. C. Su, C. S. Chang, H. L. Chen, D. L. Ho, C. S. Tsao, K. Y. Peng, S. A. Chen, *Langmuir* **2004**, *20*, 8909; W.-C. Ou-Yang, C.-S. Chang, H.-L. Chen, C.-S. Tsao, K.-Y. Peng, S.-A. Chen, C. C. Han, *Phys. Rev. E* **2005**, *72*, 031802; A. Ajayaghosh, V. K. Praveen, *Acc. Chem. Res.* **2007**, *40*, 644; P. S. Wang, H. H. Lu, C. Y. Liu, S. A. Chen, *Macromolecules* **2008**, *41*, 6500; Y.-C. Li, K.-B. Chen, H.-L. Chen, C.-S. Hsu, C.-S. Tsao, J.-H. Chen, S.-A. Chen, *Langmuir* **2006**, *22*, 11009.
[22] Y.-C. Li, C.-Y. Chen, Y.-X. Chang, P.-Y. Chuang, J.-H. Chen, H.-L. Chen, C.-S. Hsu, V. A. Ivanov, P. G. Khalatur, S.-A. Chen, *Langmuir* **2009**, *25*, 4668.
[23] J.-H. Chen, C.-W. Chiu, L.-C. Chen, S.-Y. Lai, C.-C. Lee, *Polymer* **2012**, *53*, 4843.
[24] M. Fukuda, K. Sawada, K. Yoshino, *J. Polym Sci Part A: Polym Chem* **1993**, *31*, 2465; D. Neher, *Macromol. Rapid. Comm.* **2001**, *22*, 1366; U. Scherf, E. J. W. List, *Adv. Mater.* **2002**, *14*, 477.
[25] S.-A. Chen, H.-H. Lu, C.-W. Huang, *Adv. Polym. Sci.* **2008**, *212*, 49.
[26] L.-H. Xie, C.-R. Yin, W.-Y. Lai, Q.-L. Fan, W. Huang, *Proc. Polym. Sci.* **2012**, *37*, 1192.
[27] M. Knaapila, R. Stepanyan, B. P. Lyons, M. Torkkeli, T. P. A. Hase, R. Serimaa, R. Güntner, O. H. Seeck, U. Scherf, A. P. Monkman, *Macromolecules* **2005**, *38*, 2744.
[28] M. Knaapila, R. Stepanyan, M. Torkkeli, B. P. Lyons, T. P. Ikonen, L. Almásy, J. P. Foreman, R. Serimaa, R. Güntner, U. Scherf, A. P. Monkman, *Phys. Rev. E* **2005**, *71*, 041802.
[29] M. Knaapila, M. J. Winokur, *Adv. Polym. Sci.* **2008**, *212*, 227.
[30] A. Monkman, C. Rothe, S. King, F. Dias, *Adv. Polym. Sci.* **2008**, *212*, 187.
[31] V. Marcon, N. van der Vegt, G. Wegner, G. Raos, *J. Phys. Chem. B* **2006**, *110*, 5253.
[32] B. Tanto, S. Guha, C. M. Martin, U. Scherf, M. J. Winokur, *Macromolecules* **2004**, *37*, 9438.
[33] W. Chunwaschirasiri, B. Tanto, D. L. Huber, M. J. Winokur, *Phys. Rev. Lett.* **2005**, *94*, 107402.
[34] M. Arif, C. Volz, S. Guha, *Phys. Rev. Lett.* **2006**, *96*, 025503.
[35] K. Becker, J. M. Lupton, *J. Am. Chem. Soc.* **2005**, *127*, 7306; E. Da Como, K. Becker, J. M. Lupton, *Adv. Polym. Sci.* **2008**, *212*, 293.
[36] A. J. Cadby, P. A. Lane, H. Mellor, S. J. Martin, M. Grell, C. Giebeler, D. D. C. Bradley, M. Wohlgenannt, C. An, Z. V. Vardeny, *Phys. Rev. B* **2000**, *62*, 15604.
[37] M. Brinkmann, N. Charoenthai, R. Traiphol, P. Piyakulawat, J. Wlosnewski, U. Asawapirom, *Macromolecules* **2009**, *42*, 8298; M. Knaapila, R. Stepanyan, B. P. Lyons, M. Torkkeli, A. P. Monkman, *Adv. Funct. Mater.* **2006**, *16*, 599; G. Lieser, M. Oda, T. Miteva, A. Meisel, H.-G. Nothofer, U. Scherf, D. Neher, *Macromolecules* **2000**, *33*, 4490.
[38] C. Chi, G. Lieser, V. Enkelmann, G. Wegner, *Macrom. Chem. Phys.* **2005**, *206*, 1597.
[39] C. Chi, C. Im, V. Enkelmann, A. Ziegler, G. Lieser, G. Wegner, *Chem. Eur. J* **2005**, *11*, 6833; C. Chi, C. Im, G. Wegner, *J. Chem. Phys.* **2006**, *124*, 024907.
[40] M. Knaapila, T. P. A. Hase, M. Torkkeli, R. Stepanyan, L. Bouchenoire, H.-S. Cheun, M. J. Winokur, A. P. Monkman, *Cryst. Growth Des.* **2007**, *7*, 1706.
[41] S. H. Chen, A. C. Su, C. H. Su, S. A. Chen, *Macromolecules* **2005**, *38*, 379.

[42] S. H. Chen, A. C. Su, S. A. Chen, *J. Phys. Chem. B* **2005**, *109*, 10067.
[43] M. J. Winokur, J. Slinker, D. L. Huber, *Phys. Rev. B* **2003**, *67*, 184106.
[44] S. H. Chen, H. L. Chou, A. C. Su, S. A. Chen, *Macromolecules* **2004**, *37*, 6833.
[45] M. Brinkmann, *Macromolecules* **2007**, *40*, 7532.
[46] S. H. Chen, A. C. Su, C. H. Su, S. A. Chen, *J. Phys. Chem. B* **2006**, *110*, 4007; S. Kawana, M. Durrell, J. Lu, J. E. Macdonald, M. Grell, D. D. C. Bradley, P. C. Jukes, R. A. L. Jones, S. L. Bennett, *Polymer* **2002**, *43*, 1907.
[47] M. Knaapila et al, unpublished.
[48] M. Grell, D. D. C. Bradley, X. Long, T. Chamberlain, M. Inbasekaran, E. P. Woo, M. Soliman, *Acta Polym.* **1998**, *49*, 439.
[49] C. Rothe, F. Galbrecht, U. Scherf, A. Monkman, *Adv. Mater.* **2006**, *18*, 2137.
[50] C. Rothe, S. M. King, F. Dias, A. P. Monkman, *Phys. Rev. B* **2004**, *70*, 195213.
[51] W. C. Tsoi, A. Charas, A. J. Cadby, G. Khalil, A. M. Adawi, A. Iraqi, B. Hunt, J. Morgado, D. G. Lidzey, *Adv. Funct. Mater.* **2008**, *18*, 600.
[52] A. J. C. Kuehne, M. Kaiser, A. R. Mackintosh, B. H. Wallikewitz, D. Hertel, R. A. Pethrick, K. Meerholz, *Adv. Funct. Mater.* **2011**, *21*, 2564.
[53] D. O'Carroll, I. Lieberwirth, G. Redmond, *Nature Nanotech.* **2007**, *2*, 180.
[54] G. Fytas, H. G. Nothofer, U. Scherf, D. Vlassopoulos, G. Meier, *Macromolecules* **2002**, *35*, 481.
[55] F. B. Dias, J. Morgado, A. L. Macanita, F. P. da Costa, H. D. Burrows, A. P. Monkman, *Macromolecules* **2006**, *39*, 5854.
[56] M. Knaapila, V. M. Garamus, F. B. Dias, L. Almásy, F. Galbrecht, A. Charas, J. Morgado, H. D. Burrows, U. Scherf, A. P. Monkman, *Macromolecules* **2006**, *39*, 6505.
[57] Q. Ying, B. Chu, *Macromolecules* **1987**, *20*, 362.
[58] M. H. Rahman, C.-Y. Chen, S.-C. Liao, H.-L. Chen, C.-S. Tsao, J.-H. Chen, J.-L. Liao, V. A. Ivanov, S.-A. Chen, *Macromolecules* **2007**, *40*, 6572.
[59] L. L. G. Justino, M. L. Ramos, M. Knaapila, A. T. Marques, C. J. Kudla, U. Scherf, L. Almásy, R. Schweins, H. D. Burrows, A. P. Monkman, *Macromolecules* **2011**, *44*, 334.
[60] J.-H. Chen, C.-S. Chang, Y.-X. Chang, C.-Y. Chen, H.-L. Chen, S.-A. Chen, *Macromolecules* **2009**, *42*, 1306.
[61] M. Knaapila, F. B. Dias, V. M. Garamus, L. Almásy, M. Torkkeli, K. Leppänen, F. Galbrecht, E. Preis, H. D. Burrows, U. Scherf, A. P. Monkman, *Macromolecules* **2007**, *40*, 9398
[62] D. W. Bright, F. B. Dias, F. Galbrecht, U. Scherf, A. P. Monkman, *Adv. Funct. Mater.* **2009**, *19*, 67.
[63] M.-Y. Chiu, U.-S. Jeng, C.-H. Su, K. S. Liang, K.-H. Wei, *Adv. Mater.* **2008**, *20*, 2573.
[64] M. Knaapila, R. Stepanyan, M. Torkkeli, V. M. Garamus, F. Galbrecht, B. S. Nehls, E. Preis, U. Scherf, A. P. Monkman, *Phys. Rev. E* **2008**, *77*, 051803.
[65] M. Knaapila, D. W. Bright, R. Stepanyan, M. Torkkeli, L. Almásy, R. Schweins, U. Vainio, E. Preis, F. Galbrecht, U. Scherf, A. P. Monkman, *Phys. Rev. E* **2011**, *83*, 051803.
[66] M. Surin, E. Hennebicq, C. Ego, D. Marsitzky, A. C. Grimsdale, K. Müllen, J.-L. Brédas, R. Lazzaroni, P. Leclère, *Chem. Mater.* **2004**, *16*, 994.
[67] R. Traiphol, N. Charoenthai, T. Srikhirin, D. Perahia, *Synth. Met.* **2010**, *160*, 1318.
[68] Z.-Q. Lin, N.-E. Shi, Y.-B. Li, D. Qiu, L. Zhang, J.-Y. Lin, J.-F. Zhao, C. Wang, L.-H. Xie, W. Huang, *J. Phys. Chem. C* **2011**, *115*, 4418.
[69] C. W. Cone, R. R. Cheng, D. E. Makarov, D. A. Vanden Bout, *J. Phys. Chem. B* **2011**, *115*, 12380.
[70] C.-Y. Chen, C.-S. Chang, S.-W. Huang, J.-H. Chen, H.-L. Chen, C.-I. Su, S.-A. Chen, *Macromolecules* **2010**, *43*, 4346.
[71] M. E. Caruso, M. Anni, *Phys. Rev. B* **2007**, *76*, 054207.
[72] C. C. Kitts, D. A. Vanden Bout, *Polymer* **2007**, *48*, 2322.
[73] L. Huang, X. Huang, G. Sun, C. Gu, D. Lu, Y. Ma, *J. Phys. Chem. B* **2012**, *116*, 7993.
[74] H.-F. Shi, Y. Nakai, S.-J. Liu, Q. Zhao, Z.-F. An, T. Tsuboi, W. Huang, *J. Phys. Chem. C* **2011**, *115*, 11749.
[75] D. W. Bright, F. Galbrecht, U. Scherf, A. P. Monkman, *Macromolecules* **2010**, *43*, 7860.
[76] A. Subbotin, M. Saariaho, O. Ikkala, G. ten Brinke, *Macromolecules* **2000**, *33*, 3447.
[77] R. Stepanyan, A. Subbotin, M. Knaapila, O. Ikkala, G. ten Brinke, *Macromolecules* **2003**, *36*, 3758.
[78] S. T. Milner, T. A. Witten, M. E. Cates, *Macromolecules* **1988**, *21*, 2610.
[79] M. H. Rahman, S.-C. Liao, H.-L. Chen, J.-H. Chen, V. A. Ivanov, P. P. J. Chu, S.-A. Chen, *Langmuir* **2009**, *25*, 1667.
[80] H. Cheun, F. Galbrecht, B. S. Nehls, U. Scherf, M. J. Winokur, *J. Lumin.* **2007**, *122–123*, 212.
[81] M. Knaapila, D. W. Bright, B. S. Nehls, V. M. Garamus, L. Almásy, R. Schweins, U. Scherf, A. P. Monkman, *Macromolecules* **2011**, *44*, 6453.
[82] D. W. Bright, K. C. Moss, K. T. Kamtekar, M. R. Bryce, A. P. Monkman, *Macrom. Rapid Comm.* **2011**, *32*, 983.
[83] E. Somma, B. Loppinet, C. Chi, G. Fytas, G. Wegner, *Phys. Chem. Chem. Phys.* **2006**, *8*, 2773.
[84] R. Abbel, R. van der Weegen, W. Pisula, M. Surin, P. Leclère, R. Lazzaroni, E. W. Meijer, A. P. H. J. Schenning, *Chem. Eur. J.* **2009**, *15*, 9737.
[85] J. R. Tozoni, F. E. G. Guimaraes, T. D. Z. Atvars, B. Nowacki, A. Marlleta, L. Akcelrud, T. J. Bonagamba, *Eur. Polym. J.* **2011**, *47*, 2259.
[86] M. J. Tapia, M. Monserin, H. D. Burrows, J. S. de Melo, J. Pina, R. A. E. Castro, S. Garcia, J. Estelrich, *J. Phys. Chem. B* **2011**, *115*, 5797.
[87] S. K. Lee, T. Ahn, J. H. Park, Y. K. Jung, D. S. Chung, C. E. Park, H. K. Shim, *J. Mater. Chem.* **2009**, *19*, 7062.
[88] J. Peet, E. Brocker, Y.-H. Xu, G. C. Bazan, *Adv. Mater.* **2008**, *20*, 1882.
[89] S. Moynihan, D. Iacopino, D. O'Carroll, P. Lovera, G. Redmond, *Chem. Mater.* **2008**, *20*, 996; D. O'Carroll, D. Iacopino, A. O'Riordan, P. Lovera, É. O'Connor, G. A. O'Brien, G. Redmond, *Adv. Mater.* **2008**, *20*, 42.
[90] Y. Liu, T. Murao, Y. Nakano, M. Naito, M. Fujiki, *Soft Matter* **2008**, *4*, 2396.
[91] R. C. Evans, P. C. Marr, *Chem. Comm.* **2012**, *48*, 3742.
[92] A. Charas, H. Alves, L. Alcácer, J. Morgado, *Appl. Phys. Lett.* **2006**, *89*, 143519; A. Charas, Q. Ferreira, J. Farinhas, M. Matos, L. Alcácer, J. Morgado, *Macromolecules* **2009**, *42*, 7903.
[93] A. J. C. Kuehne, A. R. Mackintosh, R. A. Pethrick, *Polymer* **2011**, *52*, 5538.
[94] M. Ariu, D. G. Lidzey, M. Sims, A. J. Cadby, P. A. Lane, D. D. C. Bradley, *J. Phys.: Condens. Matter* **2002**, *14*, 9975.
[95] M. Knaapila, L. Almásy, V. M. Garamus, M. L. Ramos, L. L. G. Justino, F. Galbrecht, E. Preis, U. Scherf, H. D. Burrows, A. P. Monkman, *Polymer* **2008**, *49*, 2033.